UNIVERSIDADE FEDERAL DA BAHIA
Curso de Pós-graduação em Geofísica

DISSERTAÇÃO DE MESTRADO

O IMPACTO DE DIFERENTES FORÇANTES NA CIRCULAÇÃO RESIDUAL DE UM ESTUÁRIO TROPICAL BEM MISTURADO: BAÍA DE TODOS OS SANTOS, BRASIL - 13ºS

RAFAEL COSTA SANTANA

SALVADOR – BAHIA
ABRIL – 2015

Documento preparado com o sistema LaTeX.

Documento elaborado com os recursos gráficos e de informática do CPGG/UFBA

O Impacto de Diferentes Forçantes na Circulação Residual de um Estuário Tropical Bem Misturado: Baía de Todos os Santos, Brasil - 13ºS

por

Rafael Costa Santana

Oceanógrafo (Universidade Federal da Bahia – 2013)

Orientador: Prof. Dr. Guilherme Lessa

Co-orientador: Prof. Dr. Carlos Teixeira

DISSERTAÇÃO DE MESTRADO

Submetida em satisfação parcial dos requisitos ao grau de

MESTRE EM CIÊNCIAS

EM

GEOFÍSICA

à

Câmara de Ensino de Pós-Graduação e Pesquisa

da

Universidade Federal da Bahia

Comissão Examinadora

_____ Dr. Guilherme Lessa

_____ Dr. Carlos Augusto França Schettini

_____ Dr. Fernando Genz

Aprovada em XX de abril de 2015

A presente pesquisa foi desenvolvida no âmbito do Grupo de Oceanografia Tropical (GOAT), com recursos próprios e com o suporte financeiro da CAPES através de bolsas de estudo.

Q999 Santana, Rafael Costa,
O Impacto de Diferentes Forçantes na Circulação Residual de um Estuário Tropical Bem Misturado: Baía de Todos os Santos, Brasil - 13°S / Rafael Costa Santana. — Salvador, 2015.
79 f.: il., mapas, fotos.

Orientador: Prof. Dr. Guilherme Lessa
Co-orientador: Prof. Dr. Carlos Teixeira
Dissertação (Mestrado) - Pós-Graduação em Geofísica. Instituto de Geociências da Universidade Federal da Bahia, 2015.

1. Bahia - Geofísica. I. Mecanismos forçantes. II. Circulação residual

911.6(813.8)(043)

Dedico esta obra à Deus, por me proporcionar uma vida cheia de amor, paz, realização profissional, muita felicidade e surfe.

Resumo

Este estudo investiga o papel de diferentes forçantes na circulação residual em um estuário tropical bem misturado: Baía de Todos os Santos (BTS). Um modelo númerico (ROMS) foi utlizado para investigar os papéis sazonais da maré, estresse do vento, fluxo de água doce, balanço de calor e vazão fluvial sobre a circulação residual da BTS. Sendo que os resultados do modelo comparam-se bem com observações de elevação, correntes, temperatura, salinidade e densidade. A maré é a principal forçante da circulação e seu fluxo residual está estruturado na entrada principal da baía com correntes direcionadas para o continente no centro do canal, e um fluxo residual de vazante próximo às margens. No entanto, a maré sozinha não é capaz de renovar substancialmente as águas da baía em 350 dias. Apesar disso, esta é responsável por forçar a exportação de água em janeiro e de junho a outubro do estuário para a plataforma, e importação nos outros meses. O vento foi importante para a circulação de superfície, forçando um fluxo no sentido oeste (norte) nos meses de primavera e verão (outono-inverno) e gerando uma inclinação do nível do mar em direção ao continente. Além disso, os efeitos do vento associados aos da maré, foram importantes na redução do tempo de descarga para 340 dias. Os fluxos de calor e de água estabeleceram uma circulação gravitacional incipiente, principalmente devido aos fortes gradientes de temperatura ($\sim$0,2 ^{o}C/km) no verão, e foram responsáveis pela redução do tempo de descarga para 147 dias devido à ação da circulação termohalina. A descarga fluvial foi a segunda forçante mais importante no controle da circulação residual nas BTS, estabelecendo um fluxo barocliníco na maior parte do estuário, incluindo a boca da BTS. Este impacto culminou na redução do tempo de descarga em 5 vezes (68 dias) em relação ao experimento simulando o efeito combinado de vento e maré e forçou a exportação de água para plataforma de maio a fevereiro. As velocidades residuais tiveram magnitudes menores do que 0,13 m s^{-1} no canal principal e foram sazonalmente controladas, com correntes mais fortes durante o verão quando ocorre o pico de descarga do rio Paraguaçu. A aceleração do gradiente pressão baroclinico é significativa nas áreas abertas da baía, distante de constrições topográficas, onde a aceleração do gradiente de pressão barotropico é equilibrada pelas acelerações advectivas horizontais.

Abstract

This study investigates the role of different forcing agent on the residual circulation in a tropical, well-mixed estuary, Baía de Todos os Santos (BTS). A numerical model (ROMS) was used to investigate the seasonal roles of the tide, wind, net heat and water fluxes and river discharge on the residual circulation in BTS. The model results compare well with observations of sea level, currents, temperature, salinity and density. The tide is the main driver of the circulation and its residual flow is structured at the bay mouth with a net-landward flow in the channel centre and a net-seaward flow on the shoulders. Although, in terms of flushing time, the tides alone were not able to reach the *e-folding time* in 350 days. Nevertheless, the tidal forcing was responsible for forcing exporting of water in January and June to October from the estuary to the shelf, and importing during the other months. The wind drag was important to the surface circulation, forcing westbound (northbound) currents in the spring-summer (fall-winter) months and generating a positive sea-level slope towards the continent. Additionally, this forcing was important in reducing the flushing time to 340 days along with the tide. The heat and water fluxes established an incipient gravitational circulation, mainly due to large ($\sim$0.2 °C/km) temperature gradients in the summer and were responsible for the reduction in the flushing time to 147 days due to the action of gravitational currents. The river discharge was second to the tide in driving the residual circulation in the BTS, and establishes the gravitational circulation through most of the estuary, including the bay mouth. This resulted in reducing the flushing time by a factor of 5 (68 days) relative to the experiment with wind and tides only and forced the exporting of water to the adjacent shelf from May to February. The residual velocities have magnitudes smaller than 0.13 m s^{-1} in the main channel and are seasonally controlled, with stronger currents during the summer when the Paraguaçu River discharge peaks. The higher baroclinic pressure acceleration is significant in the open areas of the bay away from topographic constrictions, where the barotropic pressure gradient is balanced out by the horizontal advective accelerations.

Índice

Índice de Tabelas

Índice de Figuras

1

Memorial Descritivo

O memorial descritivo disserta sobre o contexto do trabalho, apresentando os principais conceitos abordados, o estado da arte e a problemática, em seguida são ilustrados a hipótese do trabalho, o objetivo, as metodologias utilizadas e por fim os resultados mais relevantes.

1.1 Contexto teórico

A circulação residual é definida por Hansen e Rattray (1965) como o movimento resultante de uma partícula após um período de tempo igual a um ou múltiplos ciclos de maré. Está tem papel fundamental na distribuição de nutrientes, contaminantes, plâncton, sedimento em suspensão e outros materiais(Robinson, 1983). A circulação residual pode ser dividida em dois campos de forçamento. O primeiro campo é o barotrópico, o qual se divide entre o residual da maré, a diferença de elevação entre o nível do rio e do estuário, o empilhamento da água causado pelos ventos e oscilações de longo período associadas a ondas de plataforma. O segundo corresponde ao gradiente baroclínico que é resultado das variações de densidade causadas, principalmente, pela diluição da água marinha através dos rios e/ou da precipitação, concentração da mesma através da evaporação, e aquecimento ou resfriamento diferencial (Cameron e Pritchard 1963; De Silva Samarasinghe et al. 2003). O gradiente baroclínico também pode variar na escala mareal, gerando o *tidal straining*, definido por Simpson et al., (1990) como o estiramento das isopicnais durante a maré vazante.

O residual da maré é causado por interações não lineares, como a advecção, entre a onda de maré e a batimetria e/ou a linha de costa (Robinson, 1983). O vento agindo a favor das correntes de vazante tende a aumentar o fluxo tanto na superfície no mesmo sentido,

quanto promover o acréscimo de velocidade próximo ao fundo em sentido contrário, como observado por Weisberg e Zheng, (2006). O vento estuário acima tende a empilhar água na cabeceira do estuário, provocando correntes de enchente nas partes mais rasas e correntes de vazante no centro e próximo ao fundo do canal (Winant, 2004). O gradiente baroclínico clássico, associado principalmente ao gradiente de salinidade, força um circulação estuarina (ou baroclínica ou gravitacional), caracterizada por um fluxo na superfície direcionado ao oceano e outro em profundidade voltado para o continente (Cameron e Pritchard 1963). No entanto, quando as variações de salinidade são reduzidas, os gradientes de temperatura também são importantes na troca de volume entre o estuário e o oceano adjacente, como observado por De Silva Samarasinghe et al. (2003) e Teixeira (2010) em estuários temperados hipersalinos.

A investigação do papel individual de cada forçante na circulação residual pode ser executada numerica- (Li and O'Donnel 2005; Winant 2004; Weisberg and Zheng 2006; De Silva Samarasinghe et al. 2003) ou analiticamente (Reyes and Valle-Levinson 2010). No entanto, a avaliação ampla da sobreposição dos efeitos destas forçantes só pode ser realizada numericamente com o progressivo incremento da complexidade do fluxo, processo onde o número de forçantes é aumentado em sucessivos cenários de simulação numérica, possibilitando a análise do papel da forçante adicionada juntamente com as forçantes já existentes. Este procedimento foi executado por vários autores (Souto et al., 2003, Zheng e Weisberg 2004, Weisberg e Zheng 2006, Li e Li 2012, Bolaños et al 2013), para investigar os efeitos das marés, do vento e da descarga fluvial em escalas de tempo de semanas a alguns meses. Embora o estudo do impacto dos ventos soprando ao longo do eixo central do estuário tenha elucidado respostas da variação intra-anual da circulação (Zheng e Weisberg 2004; Weisberg e Zheng 2006; Li e Li 2012), não houve ainda um esforço para simular a influência do seu ciclo sazonal. Uma exceção é o trabalho de Teixeira (2010), que investigou a variação sazonal na advecção de sal e calor através da circulação baroclínica e forçada pelo vento no estuário temperado e hipersalino do Golfo de Spencer, Austrália. Também diferentemente de outros estudos, De Silva Samarasinghe et al. (2003) e Teixeira (2010) consideraram ainda os fluxos de calor e água como forçantes, identificando o importante efeito de aquecimento e resfriamento sazonais das águas interiores. A sazonalidade do fluxo estabelecida pelos fluxos de água e calor nestes estuários são fundamentais no transporte de escalares, os quais tendem a ser exportados para a plataforma durante o inverno quando a acentuação dos gradientes de densidade relacionada à queda de temperatura torna a circulação estuarina inversa mais vigorosa. A literatura carece, no entanto, de investigações sobre a importância dos fluxos e calor e de água nas correntes residuais de estuários tropicais, onde as variações sazonais tendem a ser menores.

O estudo da circulação residual também é importante para a avaliação quantitativa do grau de renovação das águas estuarinas. Esta avaliação pode ser obtida através do cálculo dos parâmetros hidrodinâmicos de tempo, tais como: tempo de residência, *e-flushing time*, tempo de descarga e tempo de exposição que considera o possível retorno das partículas durante a maré enchente (Delhez 2013). Zimmerman (1986) ao estudar o papel da maré na circulação residual evidenciou que a geração de vórtices em baía e estuários com geometria irregular tende a aumentar dispersão de partículas nessa região, o que pode levar à redução do tempo de descarga. Em relação ao circulação baroclínica, observa-se que esta tem papel fundamental na geração dos fluxos de troca, os quais contribuem substancialmente para reduzir o tempo de residência, como observado por Gross et al. (1999), Liu et al (2008) e Meyers e Luther (2008), através de modelagem numérica.

1.2 Contexto local

A Baía de Todos os Santos (BTS) é um estuário tropical, dominado por maré e bem misturado (Cirano e Lessa, 2007)(Figura 1.1). A baía está centrada em 12°50' S e 38°38' W e é a segunda maior baía do Brasil com uma de área de 1233 km^2. A BTS está localizada nas bordas da terceira cidade mais populosa do Brasil (Salvador) com cerca de 2,8 milhões de habitantes (IBGE, 2014), abriga dez terminais portuários de grande porte (Hatje and De Andrade, 2009) e a Refinaria Landulpho Alves (RLAM), os quais são potenciais fontes de contaminantes via meio aquoso. A BTS também comporta uma grande quantidade de pequenos estuários, recifes de corais e uma complexidade de ambientes sedimentares (Cruz, 2008; Barros et al., 2009), dentre os quais o fluxo de nutrientes e matéria orgânica é fundamental para a produtividade da baía.

Estuários bem misturados, como a BTS, são conhecidos por apresentar perfis de salinidade uniformes e fluxos médios unidirecionais em profundidade (Pritchard, 1955 e Cameron e Pritchard, 1963). Partindo desta premissa, Xavier (2002) estudou a circulação residual na BTS utilizando um modelo barotrópico. A autora encontrou valores máximos de velocidade do fluxo de 0,3 ms^{-1} e 0,2 ms^{-1} (médias da coluna d'água) derivados de cálculos lagrangeanos e eulerianos, respectivamente, e promediados no período de 24 h. Ambos os valores foram encontrados nas bordas do Canal de Salvador e direcionados ao oceano. Em adição, a distribuição dos vetores residuais mostra a existência de vários vórtices no interior da baía, resultantes de efeitos não lineares resultantes da interação do fluxo com a batimetria. No entanto, ao validar seus resultados com observações de 2 estações do Projeto Baía Azul, a autora constatou que seus resultados correspondiam a apenas 50% da magnitude das observações. Xavier (2002) sugeriu que tais diferenças poderiam ser atribuídas aos efeitos

baroclínicos.

Adicionalmente, a circulação residual na BTS foi estudada por Genz (2006), Cirano e Lessa (2007) e Pereira e Lessa (2009). Genz (2006) realizou levantamentos de vazão feitos com ADCP ao longo de 1 ciclo de maré no Canal de São Roque e identificou fluxos residuais

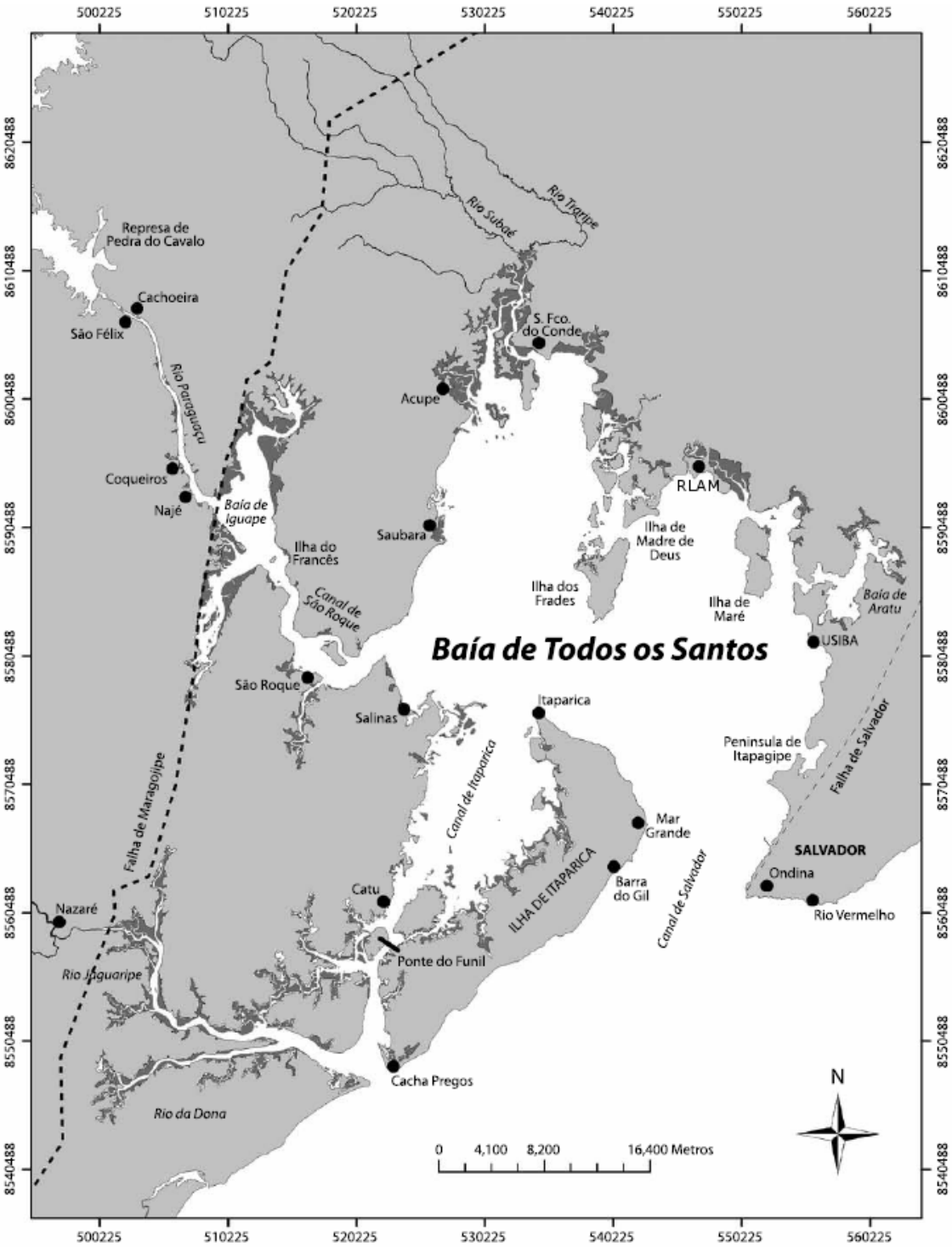

Figure 1.1: Baía de Todos os Santos e suas principais localidades. Regiões em cinza escuro representam manguezais. Extraído de Lessa et al. (2009).

de 0,02 ms^{-1} e 0,05 ms^{-1} em sizígia e quadratura, respectivamente, com estratificação lateral em sizígia e vertical em quadratura. Já Cirano e Lessa (2007), com o uso de séries temporais de 15 dias coletados no período seco e úmido pelo Projeto Baia Azul na superfície e no fundo da BTS, encontraram uma estratificação da circulação residual característica de fluxos estuarinos. Os valores da circulação residual variaram em torno de 0,05 ms^{-1} tanto para a superfície como para o fundo, com velocidades mais intensas durante a estação úmida. Por fim, Pereira e Lessa (2009), utilizando registros de ADCP com duração de 30 dias, identificaram fluxos residuais estratificados no Canal de Aratu com magnitudes de aproximadamente 0,02 ms^{-1} na estação seca e 0,08 ms^{-1} na estação úmida.

Xavier (2002) calculou, com o modelo barotrópico, que o tempo de residência máximo da BTS, associado a partículas provenientes da Baía de Iguape e Ribeira, é de 35 dias. O tempo de residência é definido como o tempo necessário para uma partícula, localizada em certa parte do domínio, deixar o estuário (Takeoka, 1984). Foi no entanto, desconsiderada a possibilidade de retorno das partículas da plataforma em direção à BTS durante as marés de enchente. Cirano e Lessa (2007) estimaram o tempo de descarga, para a região entre o fim do Canal de São Roque e a Ilha dos Frades (Figura 1.1), analiticamente através da equação descrita em Miranda et al. (2002) que considera dados de salinidade e vazão fluvial. O tempo de descarga é definido como o tempo requerido para que a concentração de uma substância, homogeneamente distribuída em um corpo d'água, seja reduzida a 37% da concentração inicial (Thomann and Mueller, 1987). Os autores encontraram valores de tempo de descarga iguais a 62 dias para o verão e 38 dias para o inverno. Apesar destes esforços, existe ainda a necessidade de investigação mais realista dos processos de troca da BTS e a plataforma, utilizando-se um modelo que permita calcular o transporte de partículas considerando os campos baroclínicos e barotrópicos da circulação.

1.2.1 Área de Estudo

A variação sazonal do fluxo de água (precipitação menos evaporação) para a BTS foi obtida através da interpolação de dados provenientes de reanálise e de diversas estações localizadas no entorno do estuário. O campo gerado mostra valores negativos de descarga para a baía de até -23 m^3s^{-1} entre setembro e fevereiro (época seca), e valores positivos que atingem 57 m^3s^{-1} entre março e agosto, representado a época chuvosa (Figura 1.2a).

A descarga fluvial aumenta em 11 vezes (124 m^3 s^{-1}) a média anual do aporte de água doce que entra na baía (Figura 1.2a). O rio Paraguaçu é detentor da maior descarga média anual (1986-2008) com o transporte de 61 m^3 s^{-1}, que deságua no lado oeste da BTS (Figura 1.1) e atinge o máximo no verão (Figura 1.2a). Um aporte de água doce mais difuso é

promovido por várias bacias hidrográficas menores localizadas em torno da baía, acumulando uma vazão média anual de 52 m^3s^{-1}, mas com um pico nos meses de outono (março-junho) (Figura 1.2a).

Como resultado do fluxo de calor, as temperaturas da superfície do mar máxima e mínima na BTS ocorrem em Fevereiro (30,0 °C) e Agosto (25,5 °C), respectivamente. A temperatura mínima é aproximadamente a mesma que no oceano, contudo, a máxima temperatura mais perto da entrada da baía é 2,0 °C menor em relação às águas mais interiores. Dessa forma, temperatura da superfície do mar experimenta amplitudes anuais de 4,0 °C no lado ocidental da baía e 2,5°C na entrada da baía, como mostrado na Figura 1.2b.

A direção média do vento na costa leste do Brasil é de ENE no verão e de SE no inverno, forçando correntes costeiras para sul e norte na plataforma, respectivamente (Amorim et al

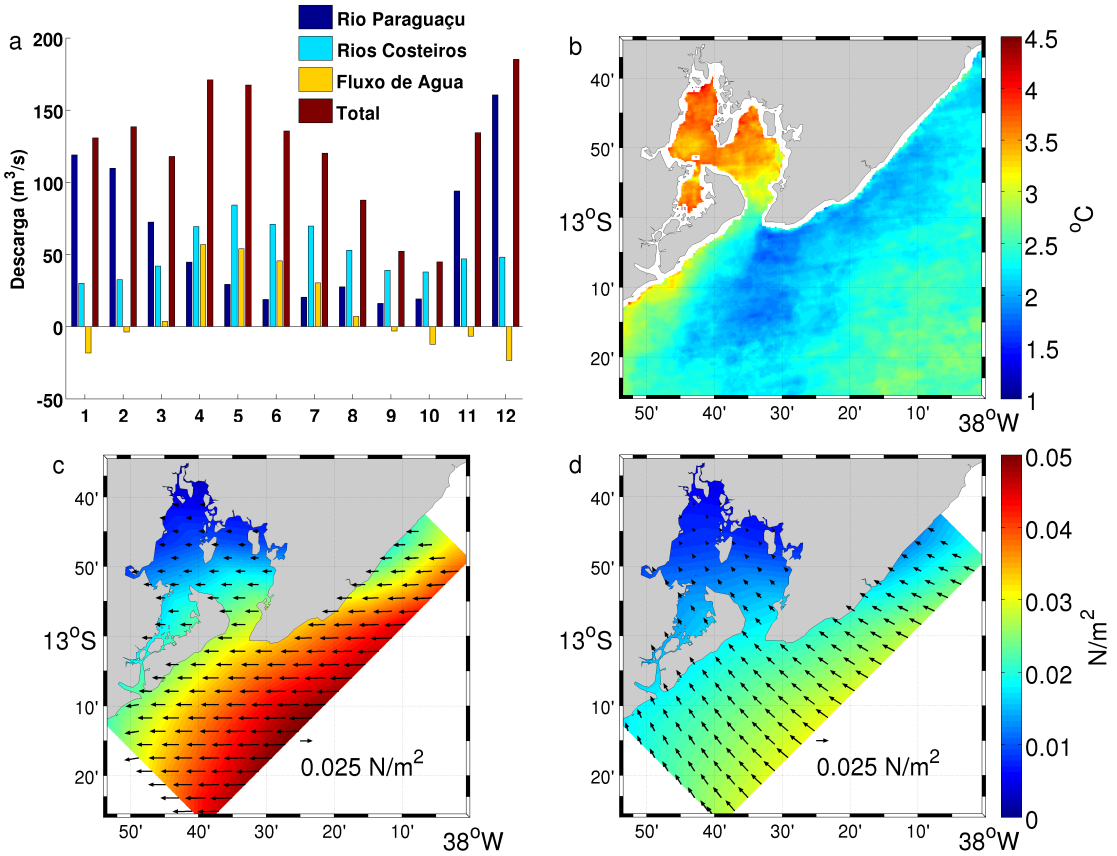

Figure 1.2: Forçantes climatológicas para a Baía de Todos os Santos. (a) Descarga do rio Paraguaçu em azul escuro, a soma dos rios e bacias costeiros em azul claro, o fluxo de água aparece em amarelo e a soma de todas as descargas se encontra em vermelho escuro; (b) variação sazonal (diferença entre médias (2003-2012) de fevereiro e agosto) da temperatura da superfície do mar; (c) estresse médio do vento (2007-2013) em janeiro obtido do CFSR (interpolado para a grade do modelo - escala de cores como em d);(d) o mesmo que (c), porém para junho.

2013). Em relação à BTS, a direção do vento tende a girar no sentido horário no interior da baía de janeiro a junho, como mostrado por Lessa et al (2009), como pode ser observado nas Figuras 1.2c e 1.2d.

As marés na BTS são semidiurnas e sofrem amplificação de cerca de 0,6 m em relação à maré oceânica. As alturas de maré na baía oscilam entre 1,87 m, em sizígia, e 0,98 m, em quadratura. Além disso, o movimento de águas na BTS é primordialmente regido pela maré, a qual éresponsável por pelomenos 86% da variância das correntes (Cirano e Lessa, 2007).

De forma objetiva, pode ser dito que a BTS é um estuário tropical dominado por maré que apresenta dois picos de aporte de água durante o ano, um em dezembro relacionado à descarga pontual do rio Paraguaçu, e outro em abril ligado ao aporte atmosférico e à descarga difusa da drenagem periférica à BTS. No verão são observados ventos de leste e um fluxo de calor positivo considerável que aquece as águas internas da baía e gera um forte gradiente de temperatura (0,2 ^{o}C/km) direcionado para o continente. Este gradiente é destruído no inverno, estação em que predominam os ventos de sudeste. Mais detalhes sobre a área de estudo são apresentados no item 2.1.3.

1.3 Hipótese do trabalho

De acordo com os resultados obtidos Li e O'Donnel (2005) utilizando simulaçãoes idealizadas em estuários curtos ($4*L/\lambda < 0.6$; onde L= comprimento do estuário, λ=comprimento da onda de maré) acredita-se que a maré na BTS forçará um fluxo residual de entrada no canal principal e correntes residuais de saída próximo as margens. A geração de vórtices pelas correntes de maré, como observado por Xavier (2002), deverá permitir um tempo de descarga relativamente curto, devido ao aumentam dos processos dispersivos (Zimmerman, 1986). O vento, por sua vez, deverá aumentar o tempo de descarga, pois as direções preferenciais tanto no inverno como no verão forçam o empilhamento de água no interior do estuário. Espera-se também que o vento force um fluxo em direção ao continente próximo às margens e um fluxo de saída no centro do canal na entrada da BTS, como observado no modelo numérico idealizado em Winant (2004). Além disso, o impacto desta forçante deve ser restrito à superfície devido aos baixos valores de tensões observadas na região. O fluxo de calor poderá ter certa importância na geração de fluxos baroclínicos clássicos no verão, quando se observa um gradiente de temperatura em direção ao continente (Cirano e Lessa, 2007). O fluxo de água (precipitação - evaporação) na estação seca deverá gerar hipersalinidades no interior da BTS, pois este é mais negativo em direção ao interior, contudo esta forçante pode favorecer a formação de uma circulação estuarina clássica na época chuvosa,

quando se observam valores positivos do fluxo. Por fim, a descarga fluvial deverá ser o maior contribuinte da geração de fluxos baroclínicos, por se constitui na maior fonte de água doce para o estuário, e seu impacto deve ser maior no verão quando o rio Paraguaçu atinge seu máximo de descarga. As forçantes baroclínicas deverão apresentar certo impacto na redução do tempo de descarga, respeitando a magnitude de cada forçante na geração dos gradientes de densidade, de acordo com os resultados de Gross et al. (1999), Liu et al (2008) e Meyers and Luther (2008).

1.4 Objetivo

O objetivo do presente trabalho é quantificar a importância de diferentes forçantes (marés, vento, fluxos de água e calor e descarga fluvial) na circulação residual da BTS acessando o impacto das forçantes sobre: a sazonalidade das trocas de volume entre o estuário e a plataforma; e o tempo de descarga.

1.5 Metodologia

As etapas realizadas na construção do presente trabalho foram:

- Revisão Bibliográfica;
- Implementação do modelo numérico Regional Ocean Modeling System (ROMS) na BTS com resolução de 500m e 20 níveis verticais;
- Calibração do modelo e de suas forçantes para simular observações características da sazonalidade da BTS;
- Validação do modelo numérico com todas as forçantes contra observações de elevação, correntes residuais e instantâneas, temperatura, salinidade e densidade;
- Análise dos resultados de circulação residual, elevação e densidade em planta; do fluxo residual ao longo do canal em seções estratégicas dentro da BTS; dos principais termos do balanço de momento para a BTS; realização dos cálculos do tempo de descarga e avaliação do impacto das forçantes sobre a troca de volume entre o estuário e a BTS nos diferentes cenários de forçamento.

Com exceção da maré, as forçantes do modelo são produtos de médias mensais, ou aqui chamadas de climatológicas. A maré é proveniente do TPXO 7.2 (Egbert et al, 1994), o

vento por sua vez é uma climatologia (2007-2013) da tensão dos ventos do *Climate Forecast System Reanalysis* (CFSR) (Saha et al. 2010). O fluxo de calor é produto do NCEP Reanalysis 2 (Kanamitsu et al. 2002), contudo, este foi corrigido para as médias (2003-2012) da temperatura da superfície do mar produzidas por Santos (2014). O fluxo de água é uma interpolação conjunta de dados de estações meteorológicas do INMET e do Projeto Bahia Azul com dados do Reanalysis 2. Por fim os dados de descarga fluvial são advindos de fluviômetros ou da literatura disponível. Mais detalhes sobre a metodologia do trabalho podem ser encontrados no item 2.1.4 (metologia do artigo).

1.6 Principais resultados

Os principais resultados do trabalho mostram que a maré é o principal agente, forçando a geração de vórtices e fortes magnitudes de circulação residual por toda a baía. Na entrada da BTS e para região localizada na metade do eixo principal, esta forçante foi responsável por gerar um fluxo horizontalmente cisalhado, marcado por correntes de entrada (saída) no centro (nas laterais) do canal. O nível d'água foi menos alterado em relação às outras forçantes, e apresentou depressões em regiões de constrição do fluxo, bancos e cabos, onde ocorreram (des)acelerações do fluxo e formação de vórtices. Como é de se esperar, a variação intra-anual da maré foi pequena, assim como a variação da circulação residual resultante. Contudo, o ciclo anual do transporte residual de volume na entrada principal foi ditado por esta forçante. Verifica-se a importação de água nos meses de verão e outono, com exceção de janeiro, e exportação de junho a outubro. Em relação ao tempo de descarga esta forçante não foi capaz de atingir o *e-folding* time em 350 dias.

O vento mostrou-se mais importante na superfície, forçando fluxos em direção à oeste (norte) no verão (inverno), que resultaram no empilhamento de água nestas regiões. Contudo, esta forçante apresentou o menor impacto na circulação residual longitudinal; em geral o impacto foi uma ordem de magnitude menor em relação às forçantes estudadas. Apesar disto, mudanças significativas foram observadas no transporte residual de volume, onde ocorreu um aumento da importação (exportação) de água no verão (inverno) pela entrada principal, tendo o oposto ocorrido no canal de Itaparica. Em conjunto com a maré, o vento consegui reduzir o tempo de descarga para 215 dias.

O fluxo de calor e fluxo de água juntos forçaram o cisalhamento vertical em algumas regiões da BTS, gerando um fluxo de saída na superfície e de entrada próximo ao fundo na metade leste da baía, principalmente no verão quando ocorrem os maiores gradientes de temperatura. As velocidades de fluxo geradas foram semelhantes às dos rios, mas seu

impacto nas trocas de água entre a BTS e a plataforma foi mínimo. Apesar disso, estes agentes forçaram a redução do tempo de descarga para 147 dias, devido à geração do fluxos de troca, principalmente na porção leste da BTS.

Os rios, juntamente com a maré, causaram as maiores modificações nos padrões de circulação da baía. Estes forçaram o aumento das correntes em direção ao oceano (superfície) e continente (fundo) já estabelecidas no experimento anterior (marés+ventos+fluxos de água e calor), e foram responsáveis pela geração de um fluxo verticalmente cisalhado por grande parte da BTS e principalmente no canal de entrada, o que reduziu o tempo de descarga para 60 dias e forçou a exportação de água de maio a fevereiro. Em adição ao fluxo de calor e o balanço de água, os rios tiveram papel importante na geração da aceleração do gradiente de pressão baroclínico que juntamente com o a aceleração do gradiente de pressão barotrópico balanceiam as acelerações da advecção horizontal e viscosidade vertical em regiões abertas da baía, distante de cabos e constrições, onde o balanço ocorre entre os termos advectivos horizontais e o gradiente de pressão barotrópico.

A complexa morfologia da baía e as mesomarés interagem no estuário para formar um diverso padrão de circulação residual, composto por vórtices e súbitas variações do fluxo. Diferentemente do que se achava há uma década atrás, os rios tem fundamental importância na geração de gradientes de densidade que proporcionam um fluxo de troca auxiliando na renovação das águas da BTS. Portanto, o uso de um modelo baroclínico é de suma importância para a simulação do transporte de material em suspensão na BTS. Inesperadamente, o fluxo de calor e o balanço de água foram responsáveis por gerar um fluxo de troca similar ao gerado pelos rios. Evidências foram trazidas que estas correntes são principalmente geradas pelo fluxo de calor no verão. Contudo, o estudo aprofundado sobre o impacto individual de cada forçante em relação ao experimento controle faz-se necessário. Para que se possa avaliar os impactos da maré e do vento na mistura/estratificação, bem como os impactos individuais do fluxo de calor e do balanço de água na circulação residual, sugere-se a utilização de uma grade mais refinada para melhor resolver a circulação na boca do canal de Itaparica e outras regiões menores da BTS. É também importante a inclusão das áreas intermareais na simulação para melhor representar os detalhes das correntes de maré.

2

Artigo

2.1 The impact of different forcing agents on the residual circulation in a tropical well mixed estuary: Baía de Todos os Santos, Brazil 13°S

Rafael Santana, Carlos Teixeira and Guilherme Lessa

Submetido à revista Ocean Dynamics.

2.1.1 Abstract

This study investigates the forcing of the residual circulation in a tropical, well-mixed estuary, Baía de Todos os Santos (Brazil). A numerical model (ROMS) was used to investigate the seasonal roles of the tide, wind, net heat and water fluxes and river discharge on the residual circulation. The tide is the main driver of the circulation and its residual flow is structured at the bay mouth with a net-landward flow in the channel centre and a net-seaward flow on the shoulders. The wind drag was important to the surface circulation, forcing westbound (northbound) currents in the spring-summer (fall-winter) months and generating a positive sea-level slope towards the continent. The heat and water fluxes established an incipient gravitational circulation, mainly due to large (∼0.2 °C/km) temperature gradients in the summer. The river discharge was second to the tide in driving the residual circulation in the BTS, and establishes the gravitational circulation through most of the bay, including the bay mouth. The residual velocities have magnitudes smaller than 0.13 m s^{-1} in the main channel and are seasonally controlled, with stronger currents during the summer when the river discharge peaks. The higher baroclinic pressure acceleration is significant in

the open areas of the bay away from topographic constrictions, where the barotropic pressure gradient is balanced out by the horizontal advective accelerations. The river discharge acting in concert with the heat and water fluxes reduced the e-folding flushing time by a factor of 5 relative to the experiment with wind and tides only.

Keywords: Residual circulation, Tropical estuary, Forcing agents and Baía de Todos os Santos

2.1.2 Introduction

Residual circulation is defined as the net movement of a particle after one or multiple tidal cycles (Hansen and Rattray 1965), and is of utmost importance in the distribution of both soluble and suspend matter (Robinson 1983). The residual circulation is forced by barotropic and baroclinic pressure fields acting in concert, but their relative importance to the resulting circulation varies in different time scales. In estuaries, the tide and the wind constitute the main barotropic forcing, and can modulate the residual circulation from tidal-, associated with tidal straining (Simpson et al., 1990), to week-, associated with higher (spring) and lower (neap) tidal stirring (Ribeiro et al., 2004), to seasonal time scales, associated with the annual oscillation of mean wind directions (Verspecht et al., 2009). The baroclinic forcing is associated to longitudinal density gradients generated by point sources of river discharge and by spatially varying heat and atmospheric water fluxes (Cameron and Pritchard, 1963; De Silva Samarasinghe et al., 2003), and are mostly influenced by the climatic seasonality.

The Baía de Todos os Santos (BTS) (Figure 2.1) is a large (1233 km^2) tropical, well-mixed estuary (Cirano and Lessa, 2007) in northeastern Brazil (13° S) subjected to intense industrial and human pressures associated with an oil refinery, 5 large commodity ports, 2 shipyards for offshore oil platforms, a Brazilian Navy base and is surrounded by the 3rd largest (population ∼4 M) metropolitan area in the country. Despite the existence of strong environmental stressors, the bay is an important fishing ground and was declared an environmental protected area by the State in 1999. Conflicting interests over an area require efficient management, and the knowledge of the structure and seasonality of the residual water circulation is crucial for determining the fate of pollutants, dredged sediments, spatial distribution of water masses, the exchange of organic and inorganic suspended matter with the shelf and the computation of residence and exposure times. Well-mixed estuaries were known to present uniform vertical salinity profiles and unidirectional stationary fluxes (Pritchard, 1955; Cameron and Pritchard, 1963), and such an understanding led Xavier (2002) to apply a barotropic 3D model to investigate the importance of the tides and winds on the residual circulation of the bay. Her results showed the existence of eddies inside the

bay, resulting from non-linear interactions between the flow and bathymetry, and lateral shear at the inlet channel induced by tides and reduced by the wind effect. The model results, however, fell short in reproducing the magnitude of the current velocities (errors up to 50%), which was attributed to non-simulated baroclinic effects.

Cirano and Lessa (2007), after analyzing an extensive set of 15-days time series of current data, reported a classical estuarine circulation both in the wet and dry seasons. Longitudinal density gradients were higher in the wet season and enhanced the gravitational circulation. Pereira and Lessa (2009) also report the existence of gravitational circulation along a 30 m deep channel leading to Aratu Bay (Figure 2.1) and called the attention to the local importance of water and heat fluxes as an incipient inversion of the density gradient was present during the summer.

The individual importance of wind, tide, river discharge, and water and heat fluxes on the residual circulation can be assessed numerically (Li and O'Donnell, 2005; Winant, 2004; Weisberg and Zheng, 2006; De Silva Samarasinghe et al., 2003) or analytically (Reyes and Valle-Levinson, 2010). However, the superposing effects of each forcing agent can be dealt with numerical simulations of incremental complexity, where the results of preceding model runs, utilizing a smaller number of driving forces, are subtracted from succeeding runs applying a higher number of forcing agents. This procedure have been followed by several authors (Souto et al., 2003; Zheng and Weisberg, 2004, Weisberg and Zheng 2006, Li and Li, 2012; Bolaños et al., 2013), to investigate the effects of tides, wind and river discharge over simulation times varying from weeks to a few months. Although the impact of up- and down-estuary winds, and upwelling and downwelling favorable winds granted a seasonal perspective to some investigations (Li and Li, 2012; Zheng and Weisberg 2004; Weisberg and Zheng 2006) there was no effort to simulate the seasonal cycle. An exception is the work of Teixeira (2010), who investigated the seasonal variation in the advection of salt and heat by the density- and wind-driven circulation of temperate hypersaline Spencer Gulf in South Australia. Also differently from the other studies, Teixeira (2010) and De Silva Samarasinghe et al. (2003) also considered the heat and water fluxes as forcing agents, identifying the important effect of the summer heating (winter cooling) of shallow inland waters in diminishing (strengthening) the density current that would otherwise have been driven (damped) by the higher (smaller) salinity gradient. Although no effort was observed in evaluate the importance of heat and water fluxes on the residual circulation of tropical estuaries.

Understanding the residual circulation is also important to the quantitative assessment of the water renewal of an estuary or calculation of hydrodynamic time parameters such as residence time, e-flushing time and exposure time (an alternative to residence time that

take into account the possible excursions in and out the control domain (Delhez, 2013). The importance of the baroclinic circulation in significantly shortening the residence time has been demonstrated by Gross et al. (1997), Liu et al (2008) and Meyers and Luther (2008) with 3D modeling. In the BTS the residence time was calculated by Xavier (2002) with a barotropic model considering the effects of winds and tides, and the longest residence time was 35 days for the most internal sectors of the bay.

This study aims to quantify the importance of five important drivers (tides, wind, heat and water fluxes and river discharge), to the residual circulation within BTS, to assess their role on the e-flushing time and to determine whether the water exchange between the bay and the continental shelf is seasonally controlled.

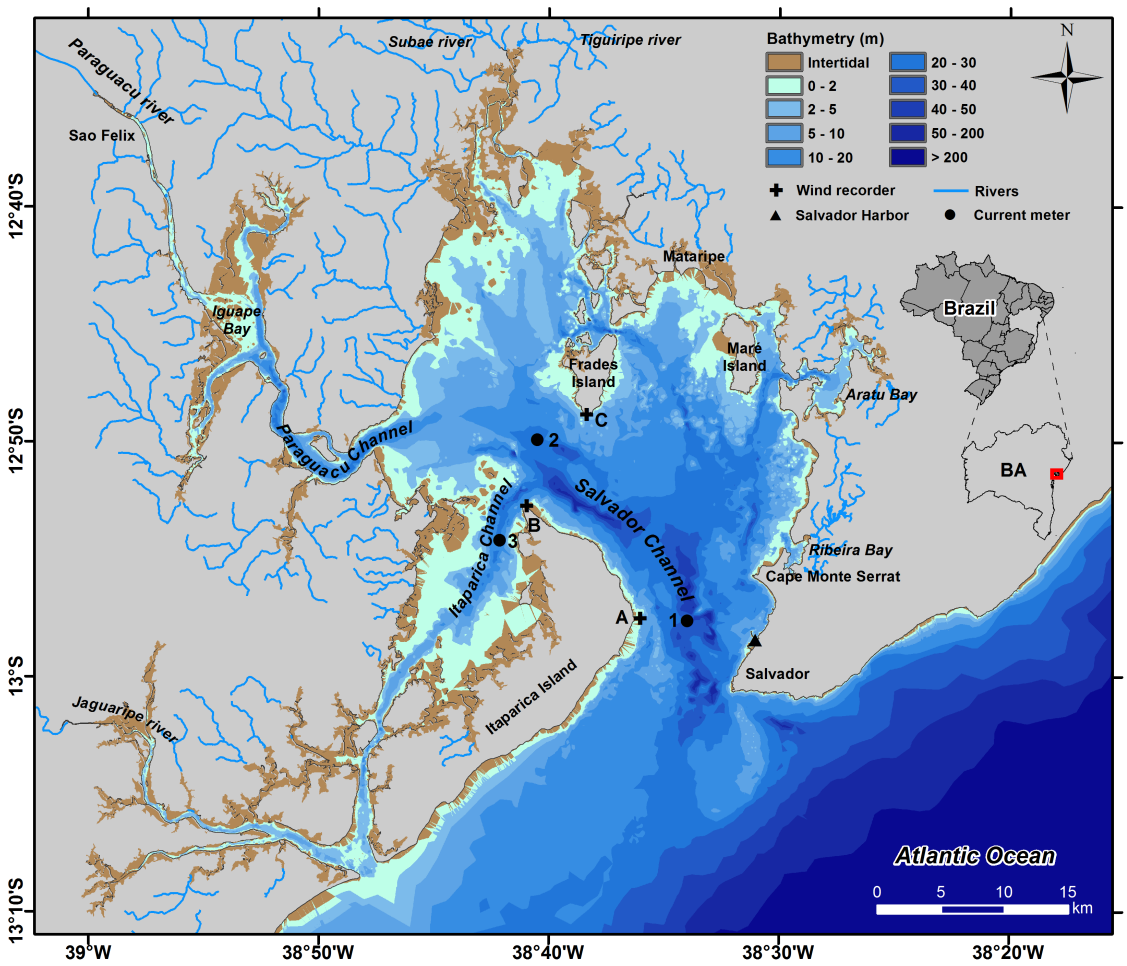

Figure 2.1: Geographical setting of the study area. Light brown shade indicates intertidal areas. Depths are nautical chart values. A, B and C indicate the location of anemometric stations used to validate the CFSR wind forcing. 1, 2 and 3 indicate the location the current meter monitoring stations. The tidal records used in the model validation were acquired in Salvador harbor (triangle) and at the location number 2 of the current meters.

2.1.3 Estuarine setting

The BTS is a tectonic estuary (Lessa et al., 2000) and as such its spatial contour is highly irregular, forming several sub-bays and dividing the central bay in a West and East segments. The area-weighted depth below the hydrographic datum is 9.8 m (Cirano and Lessa, 2007), but a 30+ m channel is incised along the main bay axis (Figure 2.1). Intertidal areas account for about 27% of the bay area.

The climate at the bay entrance is humid tropical, with mean air temperature of 25.2 °C and average precipitation and evaporation of 2100 mm and 1002 mm, respectively (INMET, 1992). Despite the annual atmospheric input of water is posite in Salvador, the northwestern part of the bay is dryer and it is located 60 km from the semi-arid, where the water balance is negative (-343 mm/year). Month-mean air temperatures vary from 30 °C in the summer to 21.3 °C in the winter. The dry season at the bay entrance (August to March) is characterized by month-mean precipitation smaller than 150 mm, whereas precipitation averages larger than 300 mm are observed between April and June. The highest evaporation is observed in January (95 mm) and the smallest in April and May (72 mm) (Lessa et al., 2009). The monthly variation of the mean surface water flux (precipitation minus evaporation) for the bay is presented in Figure 2.1a which shows negative values of up to -23 m^3 s^{-1} between September and February, and positive values reaching 57 m^3 s^{-1} between March and August.

The riverine discharge increases 11 times (124 m^3 s^{-1}) the total amount of water entering the bay (Figure 2.2a). The largest annual mean (1986-2008) inflow rate is 61 m^3 s^{-1} is from Paraguaçu River, which debouches in the western side of the bay (Figure 2.1) and reaches the discharge peak in the summer (Figure 2.2a). A more diffusive freshwater inflow is promoted by various smaller catchment areas around the bay, with an annual mean discharge of 52 m^3 s^{-1} but peaking in the autumn months (March-June) (Figure 2.2a). The total climatological fresh water discharge (surface water balance plus rivers) thus presents two maxima, one in May-June (171 m^3 s^{-1}) and another in December (185 m^3 s^{-1}), and one minimum (45 m^3 s^{-1}) in September-October (Figure 2.2a).

As a result of solar radiation, maximum and minimum SST inside the bay occurs in February (30.0 °C) and August (25.5 - 26 °C), respectively. The temperature minimum is about the same as in the ocean, but maximum SST closer to the bay entrance is 2.0 °C smaller. Therefore, SST mean annual amplitudes vary from 4.0 °C in the western side of the bay to 2.5 °C at the bay entrance, as shown in Figure 2.2b.

The mean wind direction in the northern Brazilian East Coast is from ENE in the summer and from SE in the winter, driving south and northbound coastal currents on the

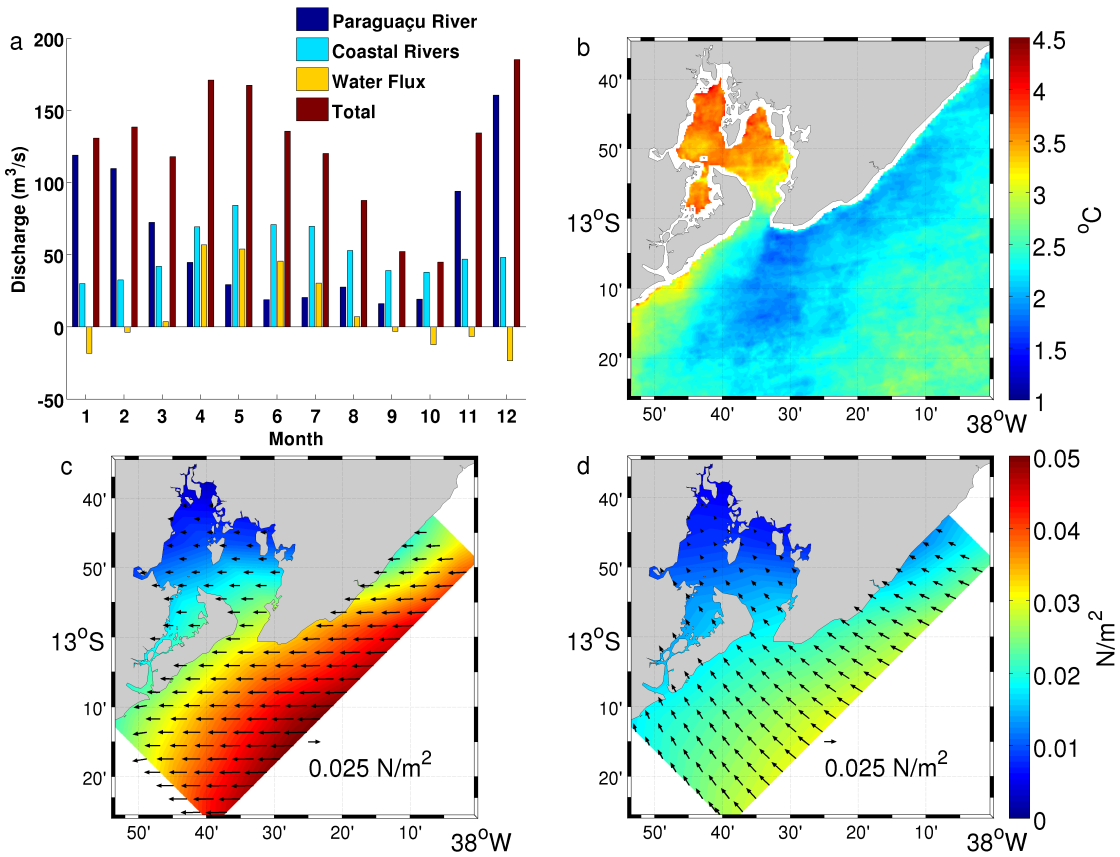

Figure 2.2: Climatological forcing agents for Baía de Todos os Santos. (a) Paraguaçu River discharge in dark blue, sum of the discharges from peripheral catchments in light blue, surface water flux (precipitation minus evaporation)in yellow and total freshwater discharge in dark red bars; (b) seasonal variation (difference between averages of February and August) of sea surface temperature; (c) mean wind stress (2007-2013) in January from CFSR (interpolated to the model grid - color scale as in d);(d) same as (c), but for the month of June.

adjacent shelf, respectively (Amorim et al., 2013). As shown by Lessa et al (2009) the wind direction tends to rotate clockwise inside the bay from January to June. Figs. 2c and 2d show the mean (2007-2013) wind stress distribution for those months as a result of interpolation of the Climate Forecast System Reanalysis (CFSR) (Saha and Coauthors, 2010) data to the model grid. The interpolation shows good correlation with wind stress data from local weather stations presented by Cirano and Lessa (2007).

The tide in the bay is semi-diurnal, with Form Number varying from 0.6 in the shelf to 0.11 in São Felix (Cirano and Lessa, 2007). The tide undergoes an average amplification of 0.6 m inside the bay, where mean spring and neap ranges are 1.87 m and 0.98 m, respectively (Lessa et al., 2009). Subtidal oscillations are small in such low latitudes, and the astronomical tides explain 97.5% of the water level variance in the center of the bay (Cirano and Lessa,

2007). Likewise, tidal currents explain 86% of the variance of the instantaneous current field (Cirano and Lessa, 2007). Significant changes in current magnitude occur between spring and neap cycles, the former being 50% faster than the latter. Tidal excursion is approximately 10 km in the lower bay during spring tides.

2.1.4 Methods

The methods present in the following sections discourse on the model implementation together with forcing data source, the numerical experiments performed to achieve the goals of the present work and the model validation against observations of the main estuarine variables.

Model setup

The numerical simulation of the circulation was performed by the Regional Ocean Modelling System (ROMS), a fully non-linear, finite difference model that uses sigma coordinates (Shchepetkin and McWilliams, 2003; Shchepetkin and McWilliams, 2005; Haidvogel et al., 2008). The grid (Figure 2.3) has a horizontal resolution of 500 m and uses 20 vertical layers, with at least 10 s-levels in the top 100 m of the water column. Grid spacing did not allow a full representation of the bay, and smaller bays and narrow segments accounting for 27% of the total area were left out. The bathymetric representation was obtained from nautical charts (resolution spanning from 1:60.000 to 1:30:000) and complemented by local field surveys over the last 15 years. The model included the maximum flooded area in spring tides, but adopted 5 m as minimum depth. The model set-up parameters are summarized in Table 2.1.

The model was initiated from rest with no elevation gradient and a vertically homogeneous water temperature and salinity fields. Initial conditions for the water temperature and salinity were set at 28 °C and 36.75 psu, respectively. The model became stable after three years of simulation (warm-up) and the results from the fourth year of simulation were used on our analysis.

Water level, external currents and salinity boundary conditions were obtained from monthly mean values (addressed here as climatological means) extracted from HYCOM/NCODA (Hybrid Coordinate Ocean Model, v. 2.2 coupled with the data assimilation system of the US Navy) (HYCOM, 2011). The HYCOM's resolution was 1/12º and the calculated averages encompassed the years 2003 to 2009. Temperature boundary conditions were obtained from a MODIS 2003-2012 SST series analyzed by Santos et al. (2014).

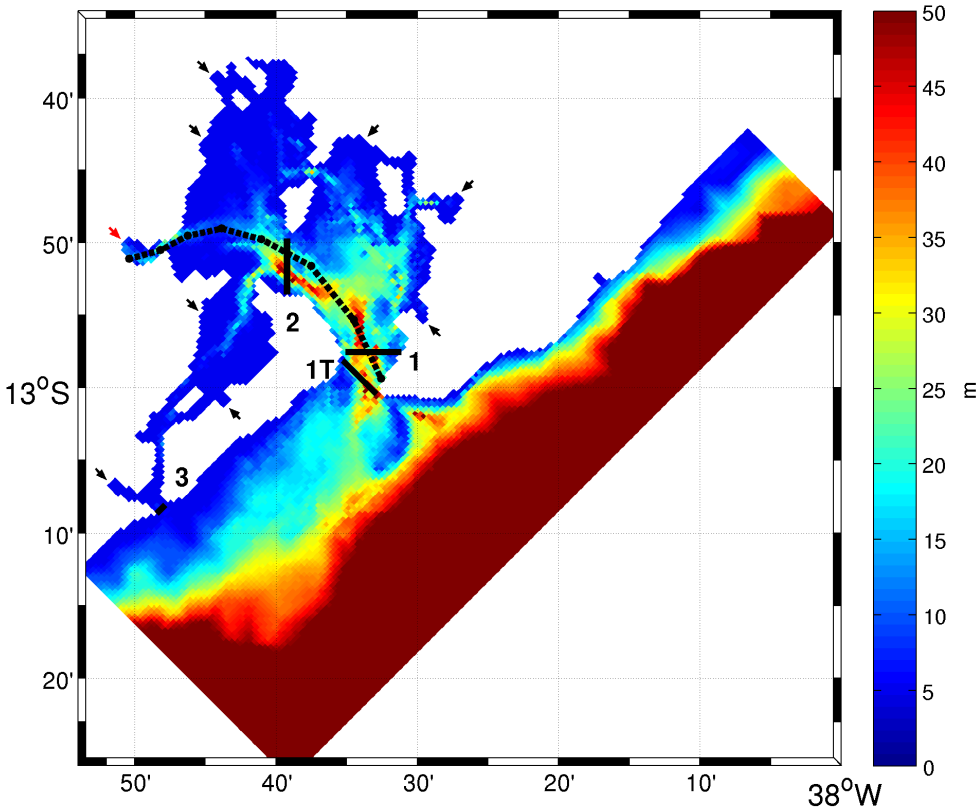

Figure 2.3: Numerical grid domain and bathymetric. Colors represent the bathymetry, regions deeper than 50 m are colored as dark red. The red arrow illustrates the Paraguaçu River discharge point source and the black arrows represent the discharge points of small tributaries. The full lines 1, 2 and 3 are transversal sections to study the longitudinal RC. The cross-sections 1T and 3 are used for volume transport computations. The dotted line represents a longitudinal section where temperature, salinity and density profiles are compared against observations

Chapman and Flather's radiation boundary conditions (Marchesiello et al., 2001) were applied to the elevation and external velocity fields, respectively, at all boundaries. Radiation plus nudging (Marchesiello et al., 2001) were used to the temperature and salinity.

In order to reproduce a stable termohaline field on the shelf, vertically homogeneous temperature and salinity profiles were used as boundary conditions. This strategy is justified by the knowledge that the shelf waters are well mixed year round, i.e., slope water with different properties apparently rarely would reach the shelf (Amorim et al., 2013).

The vertical mixing parameterization used the local closure schemes based on the Generic Length Scale (GLS) (Umlauf and Burchard, 2003) and k-kl turbulence closure scheme together with the Kantha and Clayson stability function formulation (Kantha and Clayson, 1994).

L	199	Number of points in i direction
M	179	Number of points in j direction
N	20	Number of s-levels
h_{max}	1420 m	Maximum region depth
h_{min}	5 m	Minimum region depth
θ_s	10	S-coordinates surface control parameter
θ_b	1	S-coordinates bottom control parameter
h_c	200 m	Critical depth for stretching controlling
Δx	500 m	Resolution in the zonal direction
Δy	500 m	Resolution in the meridional direction
Δt	80 s	Baroclinic time step
Δt_f	80/30 s	Barotropic time step
r	$1x10^{-2}$	Quadratic bottom drag coefficient

Table 2.1: Model setup parameters.

ROMS was forced with climatological (monthly means) values of net-heat flux, net atmospheric water flux (precipitation minus evaporation), wind stress and river discharge. The wind stress data is from CFSR (Saha et al. 2010) and the water and heat fluxes data are from NCEP Reanalysis 2 (Kanamitsu et al., 2002). The fresh water flux data from NCEP was combined with data from local meteorological stations and the heat flux data was corrected (Barnier et al., 1995) using climatological SST data from Santos (2014). The river discharge was obtained from a minimum of 21 years of fluviometry in the main tributaries (Lessa et al. 2009). The Paraguaçu River flow is related to month-mean discharges from Pedra do Cavalo dam between 1986 and 2008. The largely diffusive freshwater runoff from small tributaries (Figure 2.1) was reduced to 8 discharge points (Figure 2.3) capturing neighboring fluvial outlets, based on the data presented by Lessa et al. (2009). The tidal forcing was included in the simulations using tidal elevations and currents for the eight primary (M2, S2, N2, K2, K1, O1, P1, and Q1) tidal harmonic constituents from the regional solution of the ocean tide model TPXO 7.2 (Egbert et al., 1994).

The model produces results at a specific time step and also averages over a chosen time interval. Hourly results were used to validate the tidal simulations. All other results are based on the ROMS averages over an M2 tidal period (12.4 h).

Numerical experiments

Four experiments were conducted to investigate the role of the forcing agents to the circulation. The first experiment (EXP1) was forced only with tides, and the second (EXP2) with tides and wind stress. Both the first and second experiments will allow for the analysis of

the main barotropic forcing on the bay. The third experiment (EXP3) will simulate the effect of the atmospheric water and heat fluxes, in addition to the tides and wind, on the density field without the fluvial runoff, which will be included in the fourth experiment (EXP4). Although the simulation is climatological and not dated, a correspondence of month and tidal stage between simulated and observed data will be sought after. Table 2.2 summarizes the carried experiments.

Experiment	Tide	Wind	Heat Flux	Water Balance	River Discharge
EXP1	X				
EXP2	X	X			
EXP3	X	X	X	X	
EXP4	X	X	X	X	X

Table 2.2: Conducted simulations and corresponding forcing agents.

To assess the flushing ability of the bay in the four different dynamic scenarios, we included floats in each grid point inside the bay and followed it behavior for 350 days. The particles were positioned in the middle of the water column, irrespective of the water depth, in the fourth year of simulation. The e-folding flushing time was determined for all experiments by defining the last time the particle concentration inside the bay crossed the e^{-1}mark ($\sim$37%) of the initial concentration. Because particles are allowed to reenter the bay after being initially flushed out, the concentration varies in a tidal-time scale and the e^{-1}mark is crossed over a few times in the gradual process of concentration decay.

Model validation

In order to validate the simulations, the results from the fourth year of the more complete experiment EXP4 will be compared with the measured data and values from the literature.

The amplitude and phase of the M2, S2, O1 and K1 tidal constituents were extracted using harmonic analysis (Pawlowicz et al., 2002) from 3 years (2005 to 2007) of water level records (IBGE, 2013) collected at the bay entrance (station Salvador Harbor in Figure 2.1) and from a 2-weeks-long tidal record collected in the bay center (Cirano and Lessa, 2007 - station 2 in Figure 2.1). The model reproduced satisfactorily both amplitude and phase of the tidal elevation constituents. The deviation from observed data ([(Mod-Obs)/Obs]*100) was less than 17% in both amplitude and phase angles (Table 2.3). O1 and K1 amplitudes were correctly reproduced in both stations, as well as M2 amplitude at station 2. Only S2 amplitude at station 2, with 16% deviation, was weakly reproduced. Larger deviations are observed in the phase angles, but it is worth noticing that the main tidal carrier M2

presented the best overall fit, with an almost perfect phase match at station 2.

Constituents	Amplitude			Phase		
	Obs. (m)	**Sim. (m)**	**Dev. (%)**	**Obs. (°)**	**Sim. (°)**	**Dev. (%)**
Salvador Station						
M2	0.73	0.79	8%	221.3	222.0	0%
S2	0.24	0.26	8%	246.3	272.4	11%
O1	0.06	0.06	0%	169.1	182.3	8%
K1	0.04	0.04	0%	278.7	273.7	-2%
Station 2						
M2	0.89	0.89	0%	101.0	107.1	6%
S2	0.31	0.36	16%	121.0	127.0	5%
O1	0.06	0.06	0%	137.0	119.5	-13%
K1	0.04	0.04	0%	236.0	196.3	-17%

Table 2.3: Observed and simulated amplitudes and phase angles (referenced to the Greenwich meridian) of the four main tidal constituents and their respective model deviations. Observed and simulated values resulted from the analysis of a 2-week (Cirano and Lessa 2007) and a 3 years-long time series form Salvador station, respectively.

Hourly measurements of the along-channel current vector component were obtained for stations 1, 2 and 3 (Figure 2.1) in January and May 1999. Aanderaa-RCM7 current meters were deployed close to the surface and bottom at stations 2 and 3 for 2 weeks in January and May 1999. While a RDI-600KHz ADCP was simultaneously deployed at the bottom at station 1. Depth-average velocities were calculated and low-pass filtered to remove high frequency oscillations ($<$ 4hs) non-reproduced in the model. The observed data was compared to simulated velocities for corresponding tidal cycles in January and May, and deviation of the simulated current data was calculated as for the tidal results described above.

The average deviation for all stations and time was 14%. Station 1 presented the larger deviations, 17% and 15% for summer and winter, respectively. The model results overestimated spring-tide flood currents (Figure 2.4a, b) and the tidal asymmetry present within the BTS (ebb dominant) could not be properly reproduced. This is ascribed to the fact that the grid did not incorporated intertidal areas. At station 2 the model underestimated the velocities by less than 14%, and at station 3 the model underestimated (January) and overestimated (June) current velocities also by less than 14%.

Even though the simulations were forced by climatological means, the model was still able to reproduce the vertical profile of the residual circulation at all stations (Figure 2.5). At station 1, the two layer circulation that occurs in January was successfully replicated, with similar current velocity magnitudes and depth of the inflection point. The three layer

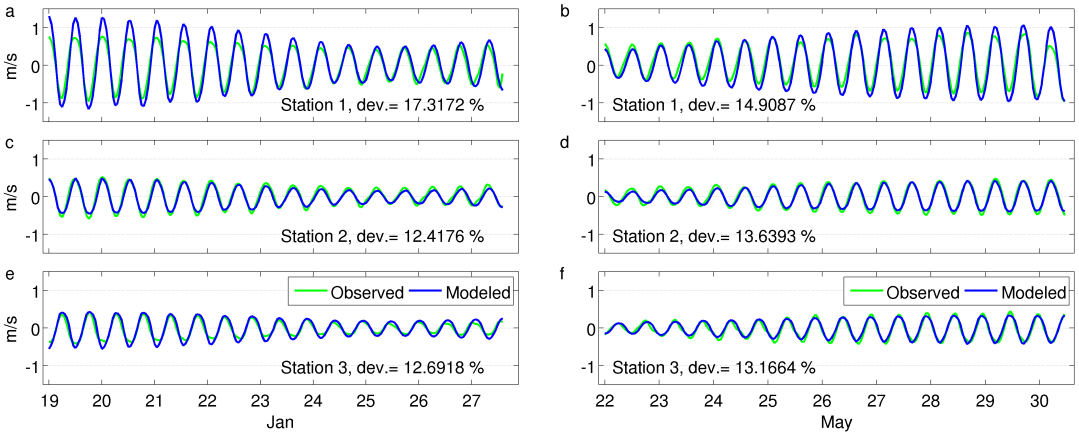

Figure 2.4: Observed and simulated depth averaged along-channel velocities at stations 1, 2 and 3 (see Figure 2.1 for location) for January and May. Positive (negative) values refer to flood (ebb) currents.

circulation that occurs in May was also reproduced, but with no corresponding velocity magnitudes nor depths of the current shear. These differences are ascribed to more intense rainfall and a strong southern wind event that occurred during the time the data was collected and are not present at the climatological monthly values used to force the model. For example, in May the mean wind stress used in the model was 0.014 Pa at station 1 and Cirano and Lessa (2007) report mean wind stresses of 0.025 ± 0.026 Pa. As for precipitation, 144 mm of rainfall accumulated in the two weeks of field observations, against 100 mm in the model.

The model reproduced well the structure of the mean vertical profile at station 2, but underestimated the velocity magnitude in the bottom and overestimated it in the surface for both months, but especially in January. The model did not reproduce satisfactorily the structure nor the current magnitude at station 3 in January, when a simulated three layer vertical profile was opposed by a unidirectional, ebb-oriented mean flow, although with some vertical shear. A better agreement exists in May when residual ebb currents were simulated below 10 m of depth. Still, the current magnitude is smaller than the observed one.

The termohaline field was validated on the basis of visual comparisons of vertical temperature, salinity and density profiles along the main bay axis (see profile location in Figure 2.3) and on the horizontal differences of these properties (Figure 2.6 and Figure 2.7). Data from January 2013 and February 2014 were used as representative of summertime conditions and data from June and July 2013 as representative of wintertime conditions. The model data was extracted along the same path of the observations and from the lowest neap tide of the respective month, although there is no correspondence of date nor time.

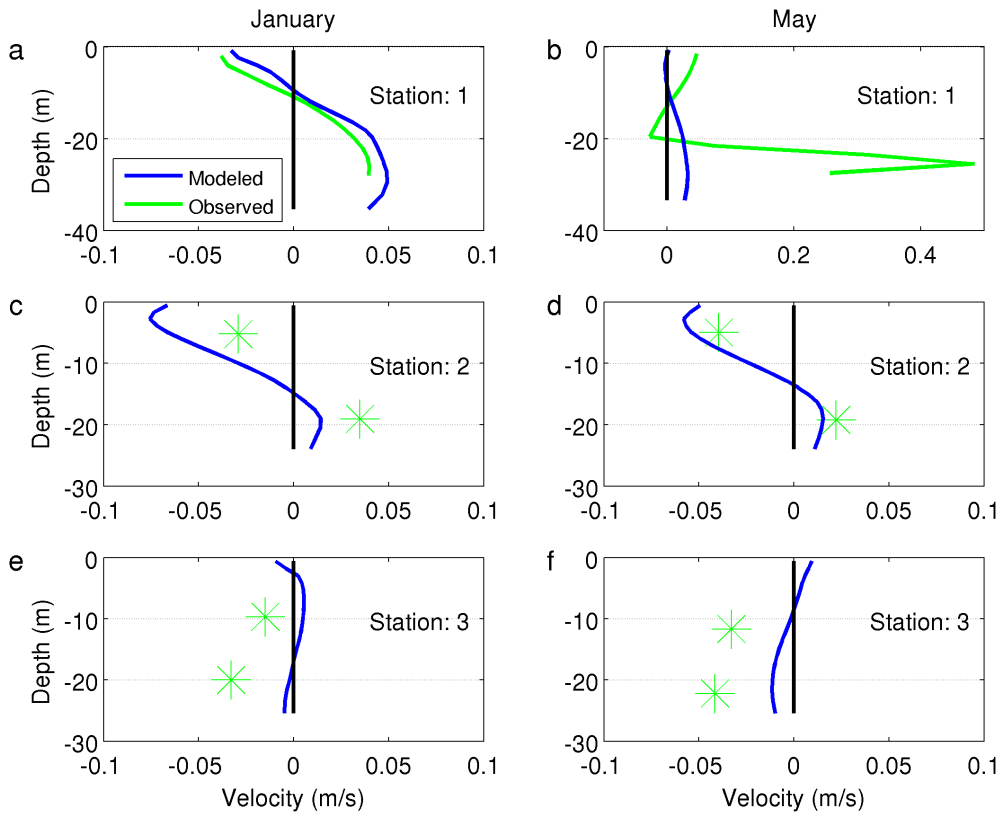

Figure 2.5: Residual circulation profiles of the observed and simulated along-channel currents at stations 1, 2 and 3 (see location in Figure 2.1) for January and May.

The simulated temperature field compares well with observed values in both summer and winter conditions (Figs. 6a, b and 7a, b). Simulated vertical mean values differ by less than 0.6 °C from observed ones, and the longitudinal temperature differences match rather well, being exactly the same (2.6 °C) in January and differing by 0.4 °C (0.5 °C against 0.1 °C). In the winter (Figure 2.7a, b) the observed temperature difference between the mouth and head of the bay in the summer is 2.6 °C both for the model and observations.

The simulated vertical mean salinities differ by less than 1.6 from observed values, and the model tended to underestimate the salinity at the head of the estuary by 0.2 (Figure 2.6c and d). The simulated longitudinal difference was stronger, however, in the summer (4.9 in the model) and agreed well with the observations (0.3 higher in the model), when the salinity field is more homogeneous, but was three times smaller in the winter (Figure 2.7c and d) (difference of 3.8 psu between the model and observations). The model underestimation of the salinity as well as the smaller salinity gradients in the winter are ascribed to negative precipitation anomalies (annual and monthly) observed in the region during field monitoring, which besides reducing the atmospheric water flux also decreased sharply the river discharge.

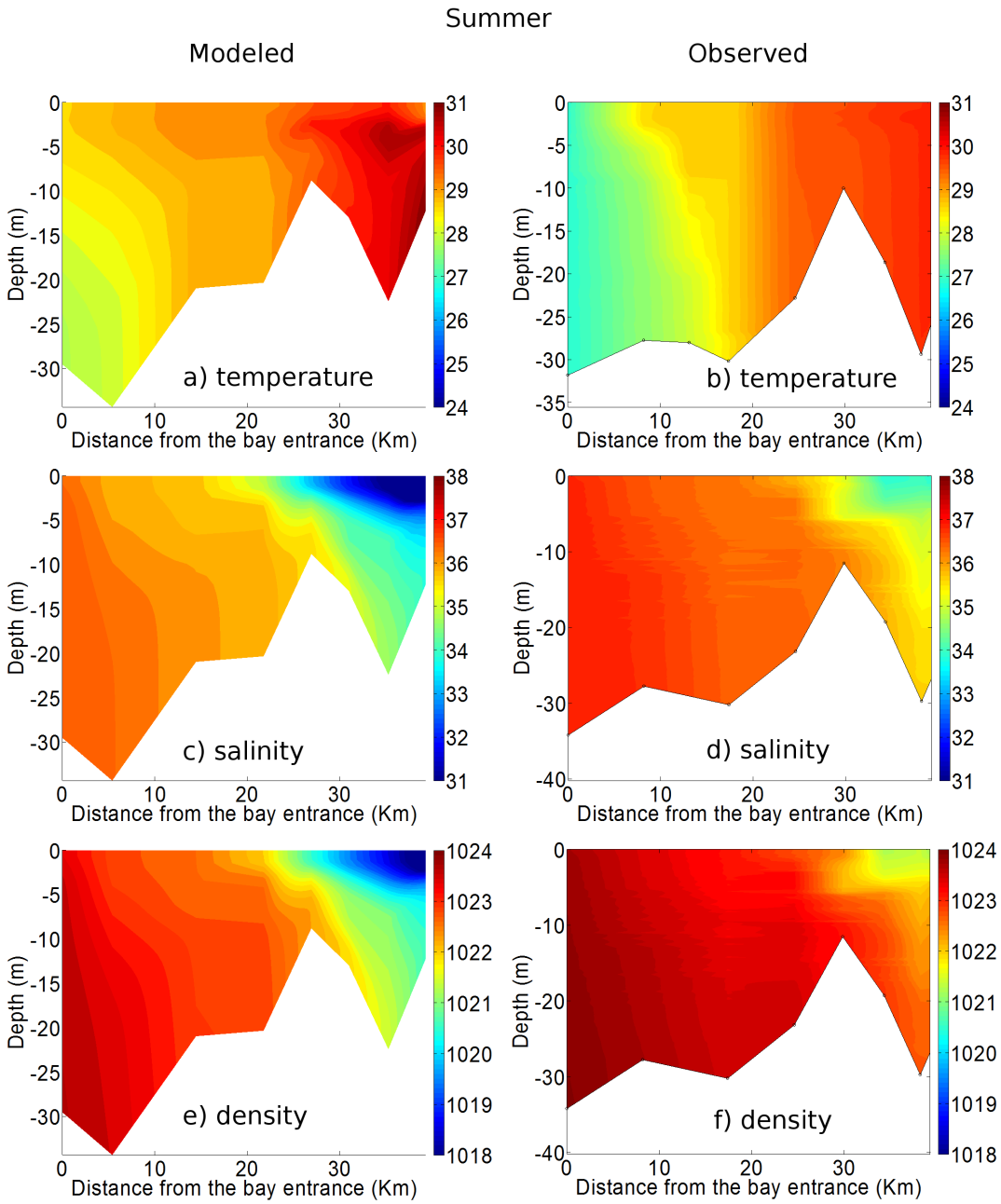

Figure 2.6: Longitudinal modeled and observed temperature, salinity and density profiles along the main axis of the BTS. (a), (c) and (e) are modeled temperature (January), salinity and density (February), respectively, at the lowest neap tide. (b), (d) and (f) are observed temperature (Jan 25 2013), salinity and density (Feb 08 2014), respectively, at neap tide conditions.

The structure of the density field was properly reproduced (Figure 2.6 and Figure 2.7 e and f), but the absolute values and gradients were compromised, especially in the summer (Figure 2.6e and f), by the discrepancies in the salinity mentioned above.

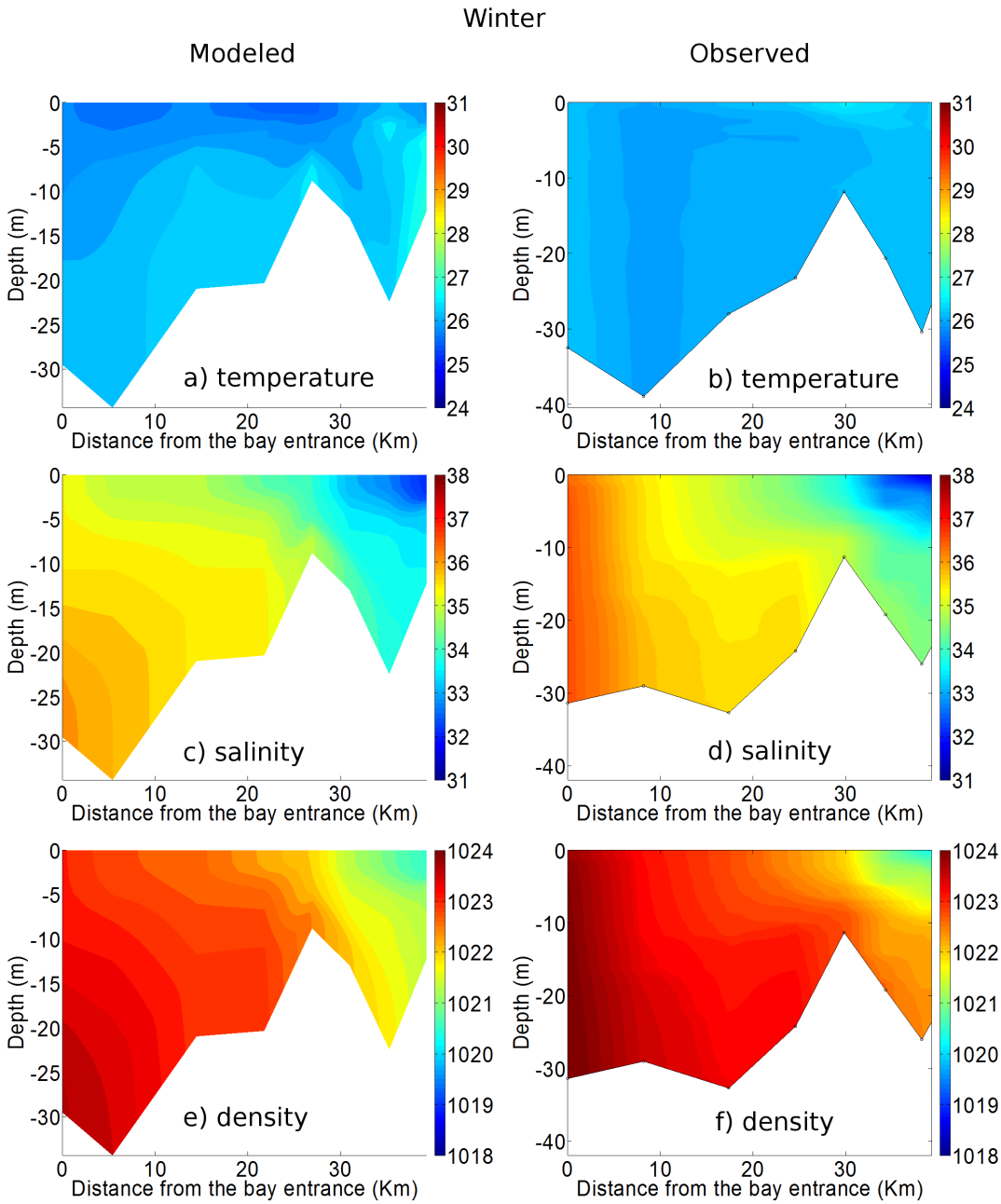

Figure 2.7: Longitudinal modeled and observed temperature, salinity and density profiles along the main axis of the BTS. (a), (c) and (e) are modeled temperature (July), salinity and density (June), respectively, at the lowest neap tide. (b), (d) and (f) are observed temperature (July 17 2013), salinity and density (June 17 2013), respectively, at neap tide conditions.

2.1.5 Results and discussion

The influence of the barotropic and baroclinic driving forces on the residual circulation was investigated based on 58 tidal cycles for the months of January and June. The results will mostly focus on the spatial distribution of the residual circulation pattern on the bot-

tom and surface layers in January and June, which are the representative months for the wet and dry seasons on the bay. We will initially present the effect of the each driving force on the eulerian residual circulation, followed by an analysis of the most important terms in the momentum equation and the flow seasonality in the control cross-sections. Finally the volume transport balance and the effect of barotropic and baroclinic forcings on the flushing time will be presented.

Residual circulation, sea-surface elevation and bottom density anomaly

The tide induced (EXP1) surface residual circulation for the dry (January) season describes a complex pattern as a result of the highly irregular bathymetric contour of the bay (Figure 2.8a). Up to six eddies can be identified, mostly with a cyclonic gyre (red circles), similarly to what was recognized by Xavier (2002). These eddies are associated with the non-linear transfer of vorticity of time-varying tidal currents to mean current field (Zimmerman, 1978). Capes and sudden expansions of channel width after narrows control eddy locations, as observed by Geyer and Signell (1990) in Vineyard Sound (MA-USA), where the residual flow tended to follow the cape's orientation. The faster(slower) velocity zones (maximum speed of 0.18 m s^{-1} at the channel inlet), are always associated with lower (higher) mean residual sea levels, that vary from a minimum of -0.04 m to a maximum of about 0 m. Overall the mean water level tends to be depressed by about 0.005m inside the bay in relation to the ocean. The maximum flow velocities around control sections 1 and 2 regions were 0.07 ms^{-1} and 0.04 ms^{-1}, ebb and flood directed, respectively.

The inclusion of the wind in the simulations (EXP2 - Figure 2.8b) creates a landward flow ($\sim$0.02 m s^{-1}) in the western part of the BTS in the summer. The process of eddy formation in- and outside of the bay remains almost unaltered(the eddy fronting Paraguaçu River disappear) but a sea-level slope is created across an E-W transect across the bay as a result of a stronger E-W flux. The water surface in the west end rises 0.01m above the mean sea level in the east side, and increases the flow exiting the bay through Itaparica channel during the summer month (as will be shown ahead). At the surface, the maximum flow velocities around control sections 1 and 2 were 0.07 ms^{-1} and 0.05 ms^{-1}, sea- and landward, respectively.

Adding heat and water fluxes to the simulations (EXP3 - Figure 2.8c) creates seaward-directed density gradients that increase the maximum velocities (ebb-directed) at the surface in cross-sections 1 (0.05 ms^{-1}) and 2 (0.09 ms^{-1}) regions. The atmospheric water flux is negative in January and turns the inner half of the BTS slightly hypersaline (not shown). However, the heat flux is highly positive and increasing water temperatures counteracts

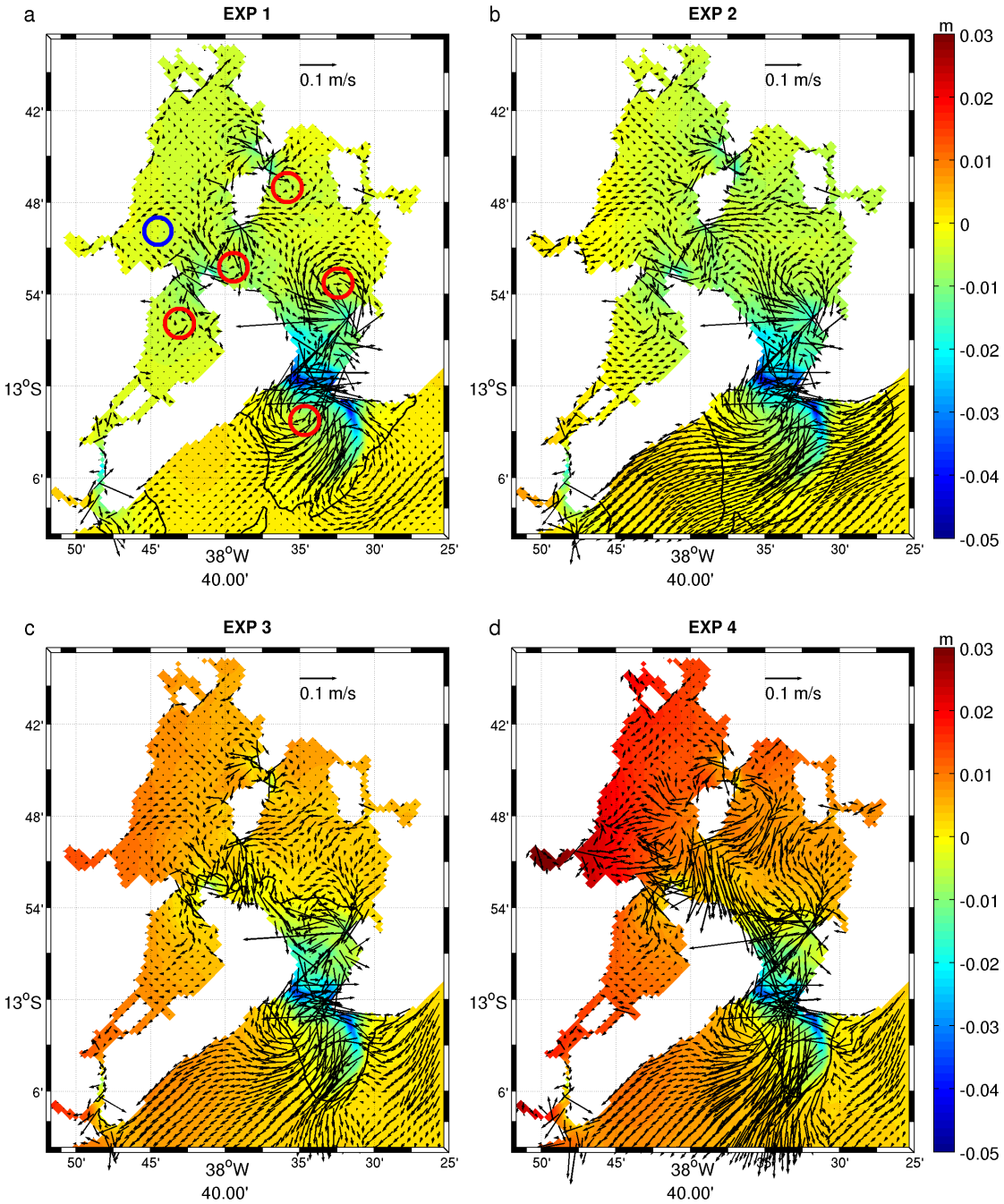

Figure 2.8: Eulerian residual circulation at the surface and water level elevation (m)for the month of January as a result of EXP 1 (a), EXP 2 (b), EXP 3 (c) and EXP 4 (d). The black line identifies the 0 m elevation contour. Red (blue) circles indicate anticyclonic (cyclonic) eddies. The results are the mean value over 58 tidal cycles for the month of January.

the effect of higher salinities and preserves an estuarine density gradient. A similar, albeit opposing, process occurs in the hypersaline bays of Southern Australia, where the inverse gravitational circulation is stifled during the summer (De Silva Samarasinghe et al., 2003)

where higher temperatures reduce the water density at the bay head. Thermal expansion of the water mass raises the water level inside the bay by about 0.01 m in relation to EXP2.

The results of EXP4 (all forcing agents - Figure 2.8d) in January show that river discharge (mainly from Paraguaçu River) step up the estuarine density gradient and enhances the maximum ebbing flow at the surface even further throughout the bay. A maximum seaward flow (0.09 ms^{-1}) is produced ahead of Paraguaçu River and its maximum velocity around cross-section 2 rises to 0.13 ms^{-1}. The addition of riverine water mass also increases the overall mean water level by another 0.01 m.

Although the resulting pattern of the surface water circulation differ amongst the four experiments, the pattern of water circulation associated with the depth-average currents for those same experiments varies little (not shown). Changes only become noticeable with EXP4, where the overall circulation is enhanced but without changing the initial pattern established by the tide.

Results for the EXP1 wet (June) season (Figure 2.9a) show no real difference in the direction and magnitude of the currents in relation to EXP 1 in January (Figure 2.8a). The water level in June was about 0,001 m lower than in January, which is ascribed to a reduction in the volume of water imported through Salvador channel, as will be shown ahead. The southern wind characteristic of this period pushes water to the north along the Itaparica Channel (0.02 ms^{-1}) and the northern cove of the bay (0.013 ms^{-1}) in EXP2 (Figure 2.9b), and slightly enhanced the anticyclonic eddy in relation to EXP1 in January. The winds also piles up water against the northern and northwestern bay shore, and mean sea level was risen by 0.008 m and 0.005 m relative to EXP1 in those respective locations.

Although June is the wet season on the coast, the positive water flux of EXP3 (Figure 2.9c) fell short in producing stronger ebbing flows relative to EXP3 in January, when the climate is dryer. Maximum current speed around cross sections 1 and 2 were reduced from 0.09 ms^{-1} and 0.05 ms^{-1} to 0.07 ms^{-1} and 0.04 ms^{-1}, respectively. This is ascribed to a spatial homogeneous temperature field that forces a smaller density gradient compared to January. Smaller water temperatures caused less thermal expansion and the mean water level was about 0.001 m lower than in January. The inclusion of river discharge in EXP4 (Figure 2.9d) increased the water level by about 0.008 m in the northern half of the bay and strengthen the ebbing flow throughout. This same process was also observed in EXP4 in January, but with a larger influence then in June, where the maximum flow speed in regions around cross-sections 1 and 2 were 0.10 m s^{-1} and 0.07 m s^{-1}, respectively. Also noticeable are the smaller maximum flow magnitudes (0.07 m s^{-1}) fronting Paraguaçu River when compared to same scenario in January, which is credited to dry season in the Paraguaçu

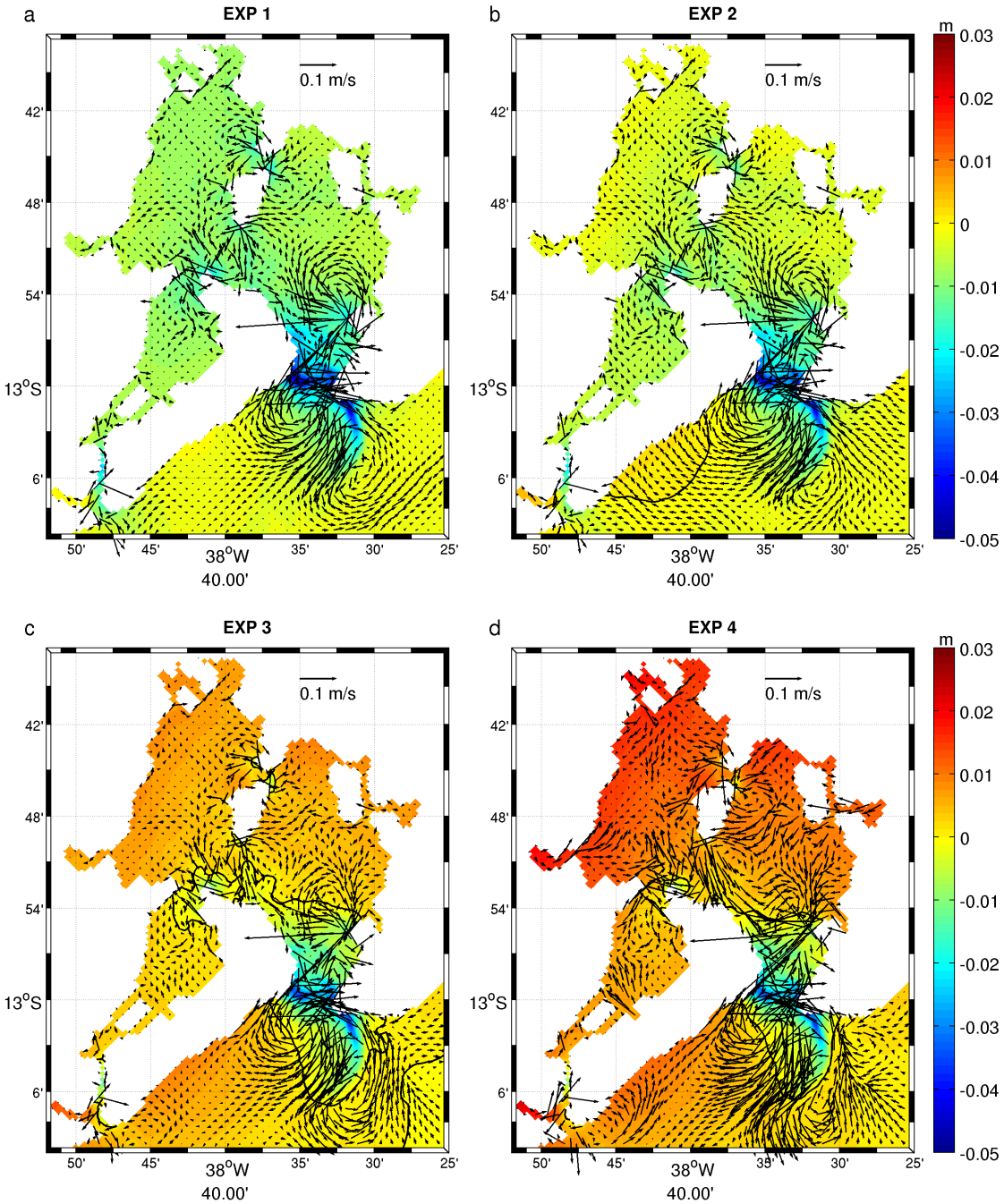

Figure 2.9: Eulerian residual circulation at the surface and water level elevation for the model domain for the month of June as a result of EXP 1 (a), EXP 2 (b), EXP 3 (c) and EXP 4 (d). The black line identifies the 0 m elevation contour. Red (blue) circles indicate anticyclonic (cyclonic) eddies. The results are the mean value over 58 tidal cycles for the month of June.

River catchment area.

The impact of heat and water fluxes plus the river discharge on the density field and

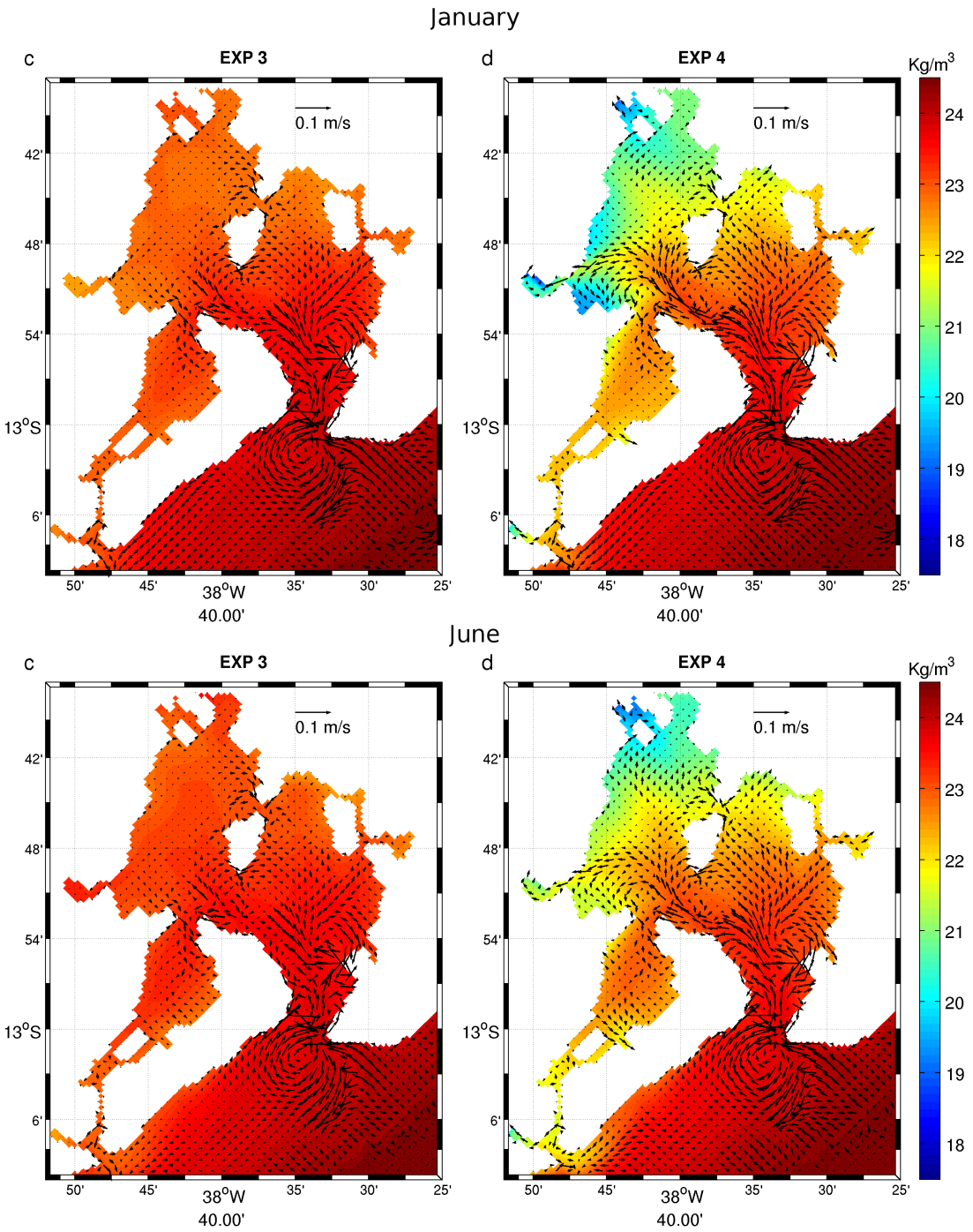

Figure 2.10: Bottom residual circulation and water density distribution for the month of January (upper panels) and June (lower panels) as a result of EXP 3 (a, c) and EXP 4 (b, d).

water circulation near the bottom is shown in Figure 2.10, again for January and June. EXP1 and EXP2 indicate the existence of flood directed currents in the middle of Salvador Channel both in the bottom (no shown) and on the surface (Figure 2.8a, b and Figure 2.9a, b). Adding heat and water fluxes (EXP3) in January (Figure 2.10a) almost doubles the

magnitude of the maximum flood currents that reach 0.05 m s^{-1}. The flood flow is pushed all the way into the estuary along the deeper channel by the negative density gradient, giving origin to vertically sheared mean flows. The strength of the flooding flow is reduced in June (Figure 2.10c) primarily because of smaller longitudinal density gradients caused by homogeneous water temperature and secondarily due to the influence of southern winds.

The addition of river discharge (EXP4 Figure 2.10b, d) produces an intensification of flood flows throughout. In Salvador Channel the velocity magnitude increases by 0.02 ms^{-1} (velocities up to 0.07 m s^{-1}), which is a similar step up of EXP3 in relation to EXP2. The river discharge has the same importance as heat and water fluxes in producing vertical shear, since flooding flow was also strengthened near the bottom with the addition of these circulation drivers. Stronger flood flows also generate a cyclonic eddy close to Paraguaçu River, which is not clearly observed on the surface. Once more smaller density gradients create less vigorous flood flows in June (Figure 2.10d).

Momentum balance

ROMS computes on every time step the acceleration terms of the 3D momentum balance, presented in Equation 2.1 for the zonal part. The first and second terms are the local and Coriolis accelerations. The remaining terms on the left-hand side are nonlinear advective accelerations, where the third and fourth terms together represent the horizontal advection, while the fifth is the vertical advection. On the right hand side, the first term is the pressure gradient (baroclinic and barotropic together), the second and third represent the horizontal and vertical viscosity. Ending the balance, the surface and bottom stresses are the fourth and fifth terms.

$$\frac{\partial u}{\partial t} - fv + u\frac{\partial u}{\partial x} + v\frac{\partial u}{\partial y} + w\frac{\partial u}{\partial z} = -\frac{1}{\rho_o}\frac{\partial P}{\partial x} + A_H(\frac{\partial^2 u}{\partial x^2} + \frac{\partial^2 u}{\partial y^2}) + A_Z\frac{\partial^2 u}{\partial z^2} + \frac{1}{\rho_o}\frac{\partial^2 \tau_s}{\partial z^2} - \frac{1}{\rho_o}\frac{\partial^2 \tau_b}{\partial z^2} \quad (2.1)$$

The results shown in Figure 2.11 are averages of 58 tidal cycles of January. The main terms of the dynamical balance of the circulation in January are the barotropic gradient and the horizontal advection. These terms stand out (Figure 2.11a, c) in regions with sudden changes in bathymetric and geometry where the confinement and acceleration of the instantaneous flow generate depressions in the mean water level (Figure 2.8 and Figure 2.9). Conversely, both terms are smaller and comparable to the baroclinic terms elsewhere (Figure 2.11b), especially close to Paraguaçu River where the baroclinic term is stronger than the barotropic and with the same direction to balance the horizontal advection (opposite direction). This illustrates a balance similar to the one presented by Scully et al. (2009),

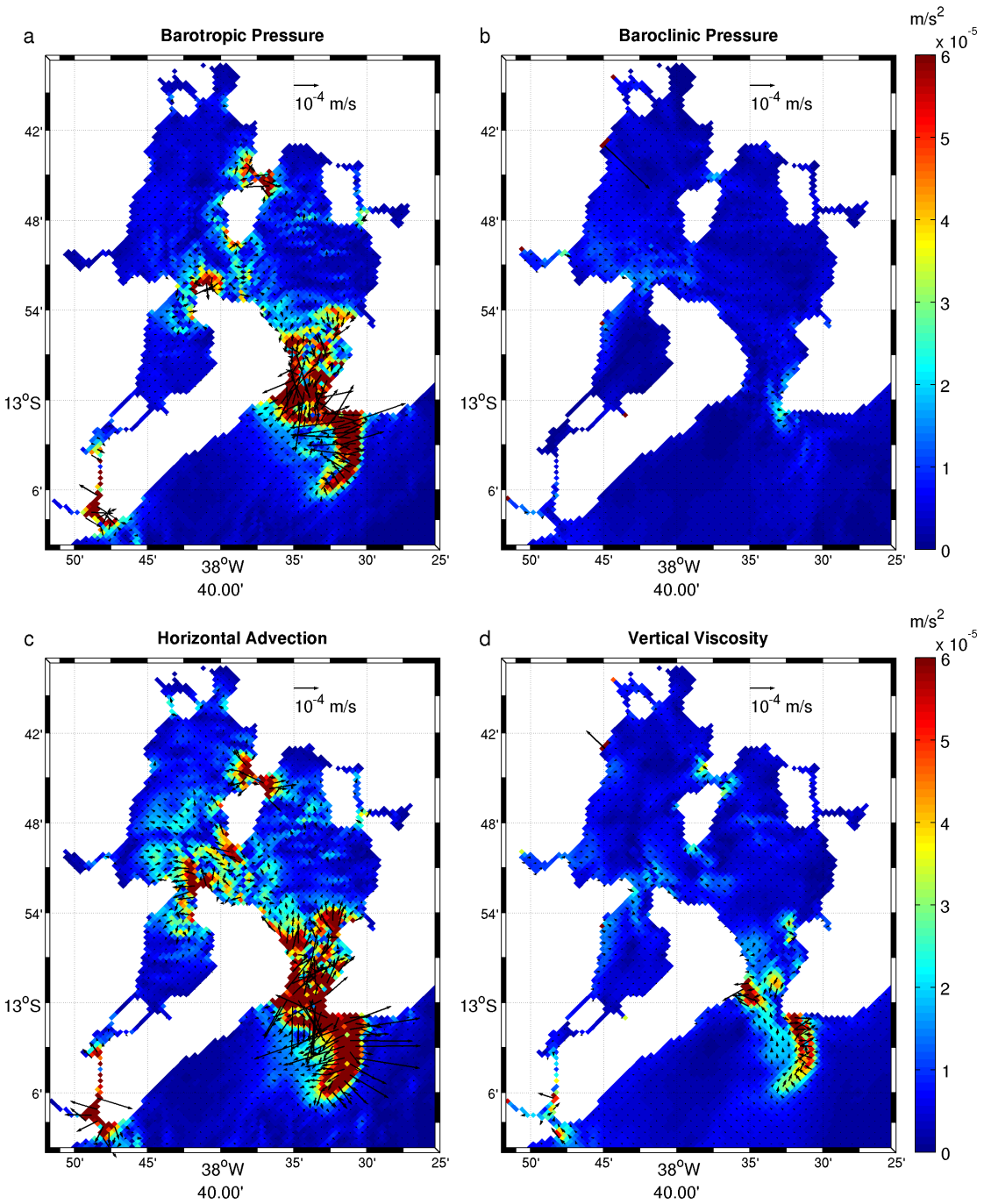

Figure 2.11: Mean acceleration of four momentum balance terms at the surface in January: (a) barotropic gradients (EXP2), (b) baroclinic gradient (EXP4-EXP2), (c) horizontal advection (EXP4) and vertical viscosity (EXP4).

who found that the advective acceleration terms act in concert with the baroclinic pressure gradient to produce movement.

In general, both the barotropic and baroclinic terms are balanced out by the viscosity

and mainly the horizontal advection terms (Figure 2.11 c, d). The latter is stronger on the surface and represents a dynamic response to sudden spatial flow (de)accelerations. The vertical viscosity generates vertical shear and is higher where current drag is stronger, i.e., on the shallows and closer to the bottom.

Because the residual current magnitude is in the order of 0.1 ms^{-1} and the inertial frequency in the bay is 3.28 x 10-5 s, the Coriolis acceleration (not shown) is about 10-6 and does not significantly influence the flow. The wind-stress is very small and also unimportant for the dynamic balance within the BTS (not shown).

Along-channel residual circulation

The impact of each forcing agent on the magnitude and structure of the along-channel residual flow was investigated at cross-sections 1 and 2 (see Figure 2.3 for location), respectively at the entrance and middle of the bay. The results of EXP1 (Figure 2.12a) for January in cross-section 1 show a horizontally stratified flow, with water flowing into the bay through the thalweg in the centre (maximum velocity of 0.04 m s^{-1}) and ebbing through the shallower margins (maximum velocity of 0.06 m s^{-1}). These results are in close agreement with numerical simulations performed by Xavier (2002) in BTS and by Li and O'Donnell (2005) in an idealized short estuary ($4*L/\lambda < 0.6$; where L= estuary length, λ=tidal wave length), which is the case of the BTS. The wind has no effect on the flow structure engendered by the tides alone (Figure 2.12b). The inclusion of heat and water fluxes in EXP3 (Figure 2.12C) generate a small vertical shear in the flood flow as the bottom (surface) velocities increase (decrease), and an intensification of the ebbing flow on the left margin. The residual flow structure is, however, drastically modified with the inclusion of the river discharge in EXP4 (Figure 2.12d), where the initially horizontally stratified flow becomes vertically stratified and an increase of about 0.02 m s^{-1} is observed in both flood and ebb velocity maxima.

The results for June (not shown) are very similar for EXP1, EXP2. When the water and heat fluxes (EXP3 - Figure 2.12e), as well as river discharge (EXP4 - Figure 2.12f), are included in the June simulations, during the maximum water flux into the bay, a smaller degree of velocity shear is present compared with January. In both cases this is a result of the smaller longitudinal density gradient and the local effect of southern winds blowing longitudinally to the cross section.

Akin to cross-section 1, a horizontally stratified flow is also established by the tides in cross-section 2 (EXP1) (Figure 2.13a), with the development of flood currents in the deepest segments of the cross section. Maximum flood and ebb velocities of about 0.03 m s^{-1} and -0.01 m s^{-1}, respectively, or about half the value of cross-section 1.The inclusion of the wind

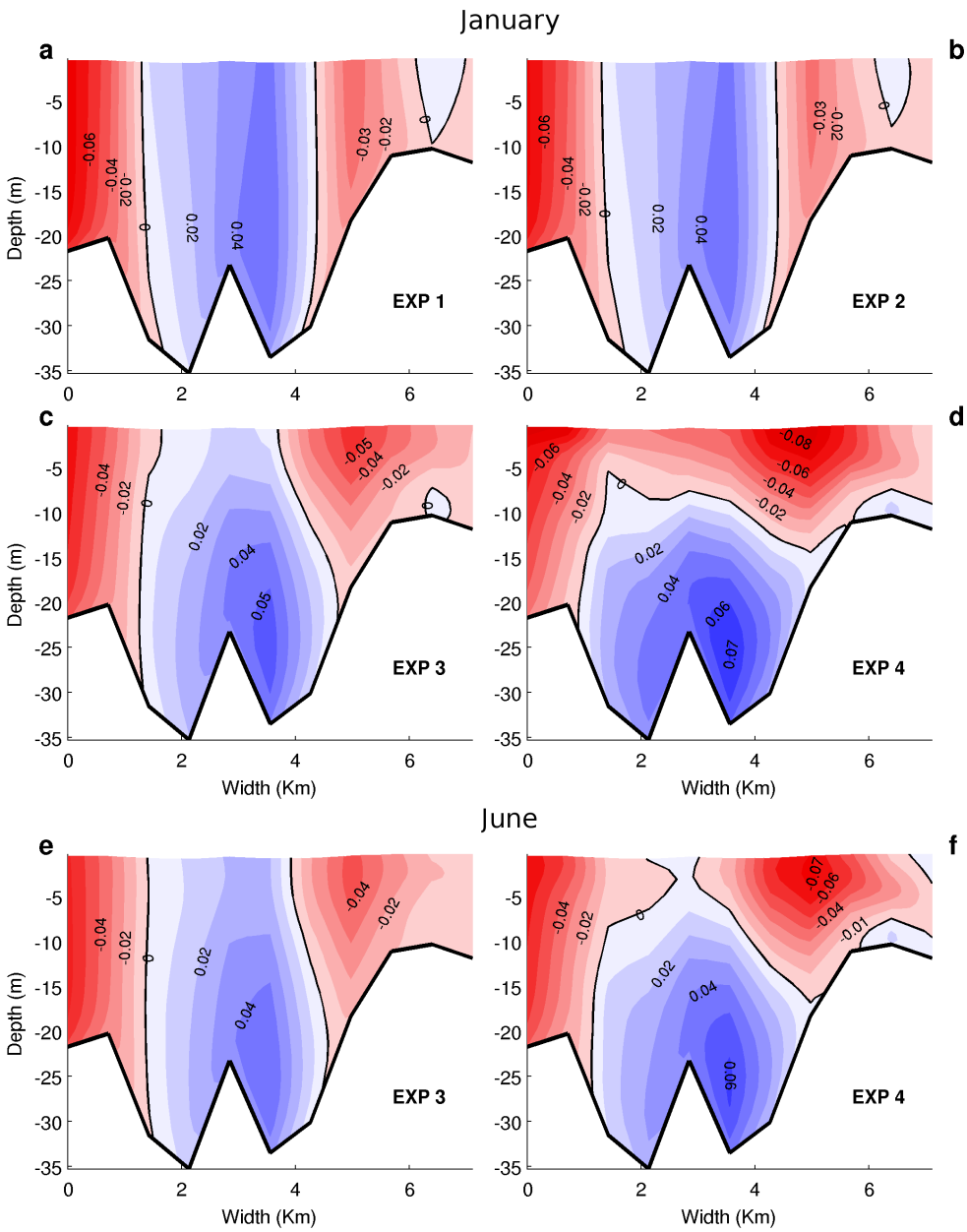

Figure 2.12: Residual circulation at cross-section 1 (looking into the estuary) for January (a - EXP1, b - EXP2, c - EXP3, d - EXP4) and June (e - EXP3, f- EXP4). Positive (blue) flows denote inflow, whereas negative (red) flows denote outflow.

effect (EXP2 - Figure 2.13b) does not alter the initial structure, but increase the maximum flood current velocities to 0.04 m s^{-1}. It also generates some shear in the ebbing flow, as the wind stress drags surface water upstream. The inclusion of the heat and water fluxes (EXP3 - Figure 2.13c) enhances the ebbing flow magnitude by 0.02 m s^{-1}, and the flow becomes again horizontally stratified. The flood currents, however, take over the thalweg. Adding river discharge (EXP4 - Figure 2.13d) practically increase the flood and ebb velocities three

fold, with velocity maximum of 0.07 m s^{-1} and 0.08 m s^{-1}, respectively. The flow continues to be horizontally stratified, but apparently more as a result of the geometry of the cross section.

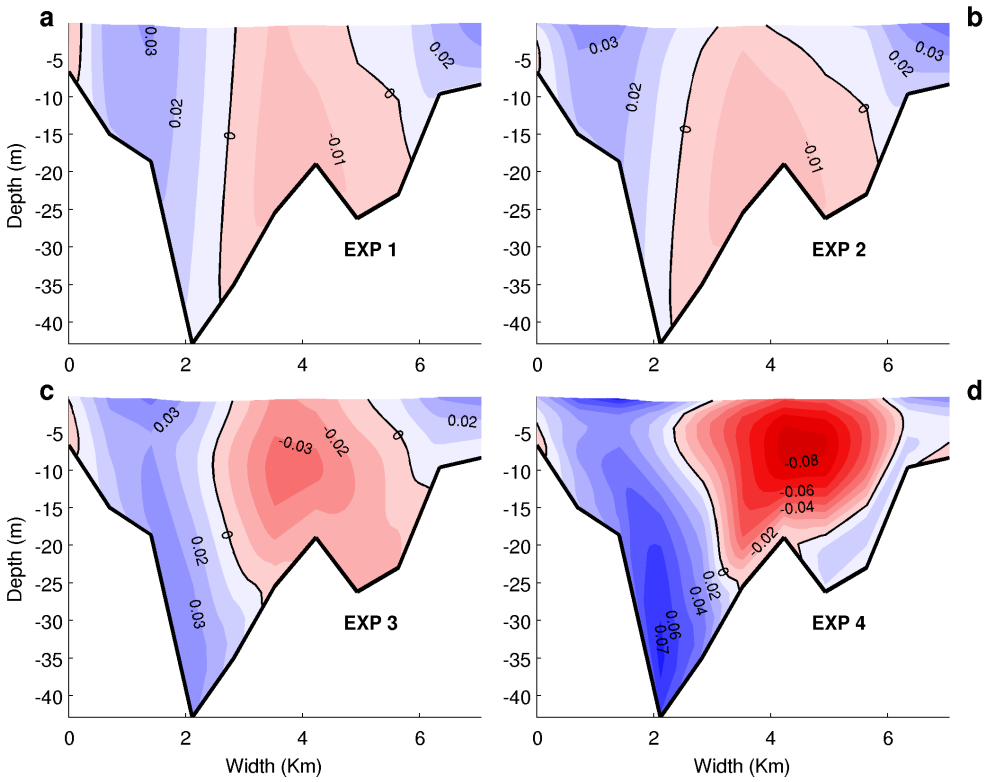

Figure 2.13: Residual circulation at cross-section 2 (looking into the estuary) in the months of January (a - EXP1, b - EXP2, c - EXP3, d - EXP4) and June (e - EXP3, f - EXP4). Positive (blue) flows are flood oriented, whereas negative (red) flows are ebb oriented.

To isolate the impact that the insertion of each forcing agent (wind, heat and water fluxes, and river discharge) causes to the circulation, the results of a preceding experiment was subtracted from the succeeding one (Figure 2.14). For instance, the wind effect was isolated by subtracting the residual along-channel flow of EXP1 from EXP2. Figure 2.13b shows that the wind in January causes a horizontally sheared flow that opposes the one produced by the tides alone, with an outgoing flow in the center and an incoming flow through the sides with similar magnitude (0.02 ms^{-1}). It is surprising to see that the heat and water fluxes (Figure 2.14c) and the river discharge (Figure 2.14d) produce vertically sheared flows with similar magnitude (maximum $\sim$ -0.03 m s^{-1} and 0.01 m s^{-1}) and degree of shear (the flow stratifies between 10 and 15 m of depth). The magnitude of the maximum wind generated flow at the bay entrance in June (not shown) is twice as strong as in January (or 0.04 m s^{-1}), but its structure remains the same. Likewise, vertically sheared flows with

similar magnitudes are associated to water and heat fluxes and river discharge, but the velocities are about 0.01 m s^{-1} slower than in January. This weaker baroclinic circulation is due to smaller longitudinal density gradients caused by the heat and water fluxes and to a river discharge more evenly distributed around the bay at the same time the outflow from Paraguaçu River is at its lowest.

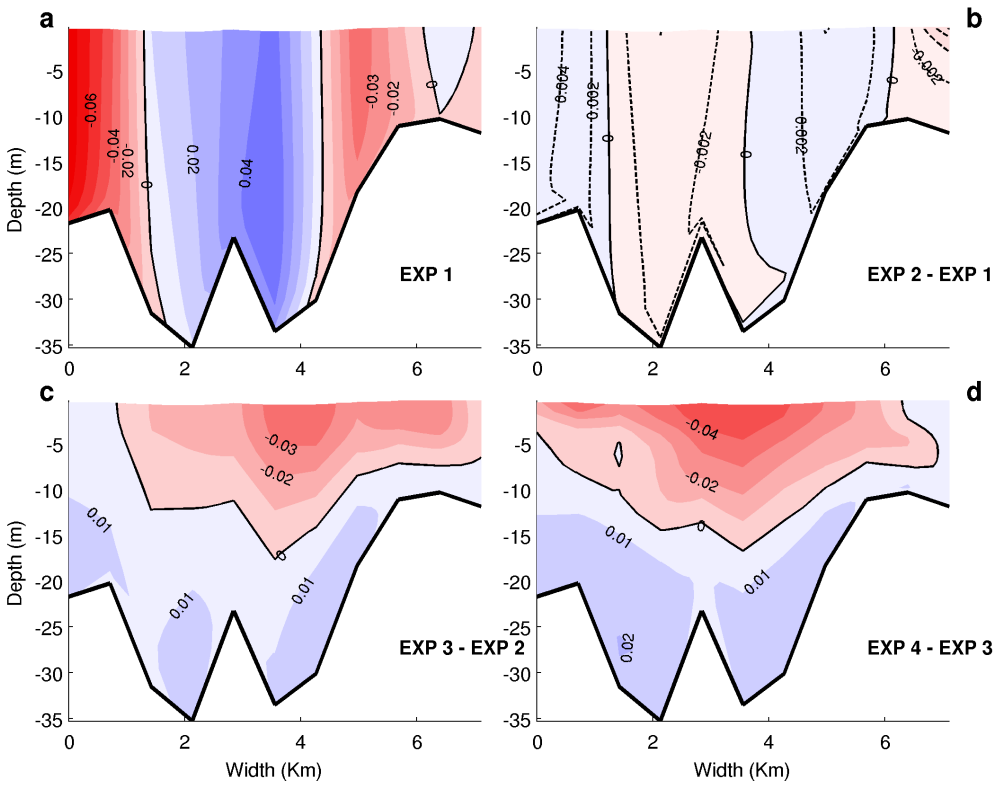

Figure 2.14: Magnitude and structure of the residual flow at cross-section 1 (looking into the estuary) at the bay entrance induced by the tides (a), wind (b), heat and water fluxes(c) and river discharge (d) for the month of January. Positive (blue) velocities are flood oriented.

In cross section 2 the January wind blowing perpendicular to the cross section creates a vertically stratified flow one order of magnitude slower than the tide (Figure 2.15b). This structure fits well with Winant's (2004) barotropic model results for the mid-section an idealized elongated basin. The flow forced by heat flux and water fluxes is strong as the tidal residual (Figure 2.15c), and also with similar magnitudes to the one engendered at cross section 1. The flow tends to become vertically stratified, with maximum flood currents taking place at the bottom of the thalweg, but a weak horizontal stratification still exists. Given the closer proximity, the impact of the river discharge on cross section 2 is much stronger than that in cross-section 1 (Figure 2.15d). Although flood currents have equal magnitudes (maximum of 0.03 m s^{-1}), the ebb flow is about three times faster (0.06 m s^{-1}) than that

driven by the water and heat fluxes. The conditions in June (not shown) are quite similar to January's, with main differences associated to a unidirectional, flood-oriented, wind-driven current with magnitudes of 0.002 m s^{-1} and smaller current magnitudes (maximum of 0.04 m s^{-1}) associated to a less important Paraguaçu River discharge.

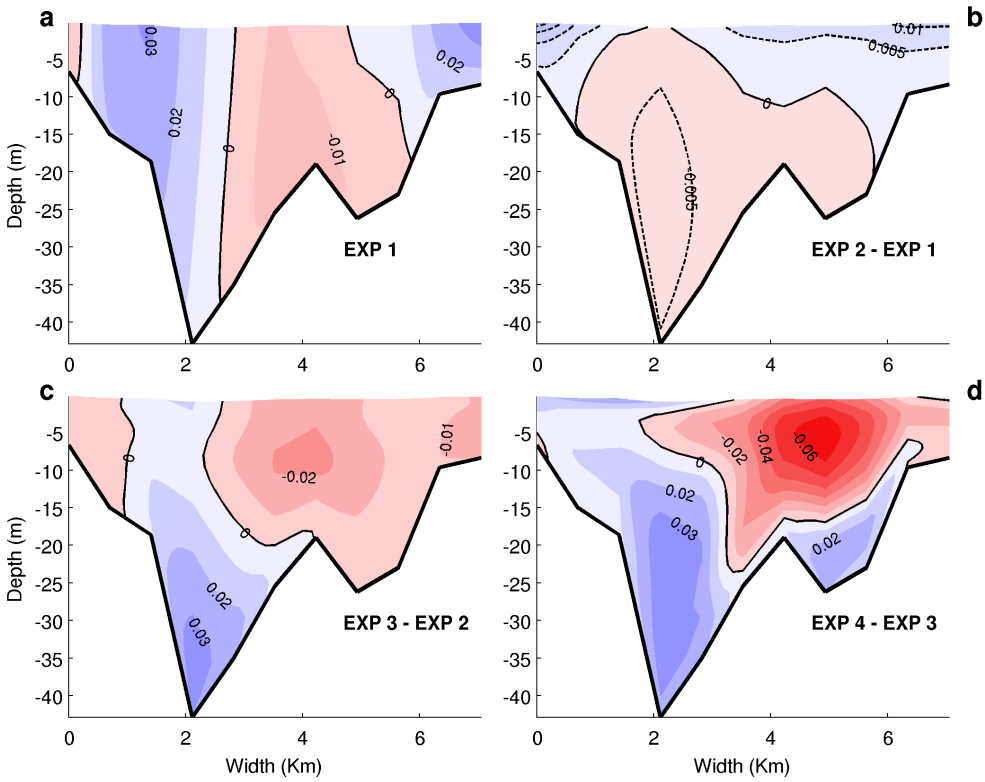

Figure 2.15: Magnitude and structure of the residual flow at cross-section 1 (looking into the estuary) at the bay entrance induced by the tides (a), wind (b), heat and water fluxes(c) and river discharge (d) for the month of January. Positive (blue) velocities are flood oriented.

Cirano and Lessa (2007), after analyzing an extensive set of 15-days time series of current data, reported a classical estuarine circulation both in the wet and dry seasons. However, the authors found higher longitudinal density gradients, and enhanced gravitational circulation, in the wet season, which is contrary to the seasonality observed with climatological means. This shows that inter-annual variations in climate induce important changes in the circulation. By the same token, Pereira and Lessa (2009) indicate that spatial variations in water density might propel different modes of circulation in sectors of the bay. The authors report the existence of an occasional inverse gravitational circulation along a 30 m deep channel leading to Aratu Bay (Figure 2.1), calling the attention to how the local water and heat fluxes in the summer can invert the density gradient between the Aratu Bay and the BTS.

Residual volume transport

Discharge computations between the bay and the ocean were performed at cross-sections 3 and 1T (Figure 2.3). The use of another cross-section at the main bay entrance was necessary given the need to align the cross section with the mesh grid for computations within ROMS. The results (Figure 2.16) show that the month-mean residual discharge varies seasonally and that an anti-clockwise residual flow may exists around Itaparica Island as suggested by (Cirano and Lessa, 2007), with positive (flooding) flows prevailing in Salvador Channel and negative flows (ebbing) occurring mainly through Itaparica Channel. The tidally driven flow (EXP1) causes an almost constant (interrupted only in July) inflow of water through cross section 1T and a perennial outflow through cross section 3 (Figure 2.16). The month-mean discharges in cross section 1T vary from 420 m^3 s^{-1} in April to -20 m^3 s^{-1} in July. An almost constant month-mean discharge of about -200 m^3 s^{-1} is observed in cross section 3. The net balance of the tidally-driven flow (Figure 2.16) shows that the bay imports water between November and May (except January) and exports between June and October. This modulation is caused by the lunisolar, semi-diurnal constituent K2 that modulates the amplitude and frequency of S2 for the declination of the sun (Pugh, 1987). The intra-annual variation shown in Figure 2.16 varies from year to year as it was verified in a 10 years long flow simulation in the BTS due to a different interannual tidal forcing. The annual discharge budget equals to -1.97 m^3 s^{-1}.

The results of EXP2 and EXP3 show a similar seasonal trend to EXP1, but with an extended period of landward directed discharge in cross section 1T (June to August) and a corresponding reduction of the seaward directed discharges at cross section 3. The net-month discharge balance (Figure 2.16) does not show any difference to the tidally-driven flow. However, increasing landward (seaward) discharges in cross section 1T (3) causes a progressive reduction in the net-annual landward discharge, which show net discharges of -1.57 m^3 s^{-1} in EXP 2 and -1.36 m^3 s^{-1} in EXP3). Therefore the net heat and water fluxes do not cause any significant additional effect on the discharge budget modified by the wind.

Again significant changes occur in the magnitude of the discharge budget with the inclusion of the rivers (Figure 2.16). The water outflow between June and August in both cross sections is enhanced, while the landward (seaward) directed mean discharge through cross section 1T (3) is reduced (enlarged) in the other months. Smaller changes occur in September (a reduction of just $\sim$20 m^3 s^{-1} in cross section 1 when compared to $\sim$150 m^3 s^{-1} in December) when there is the second smallest total freshwater discharge to the bay. The net-month discharge balance (Figure 2.16) shows that net-landward discharges occurs

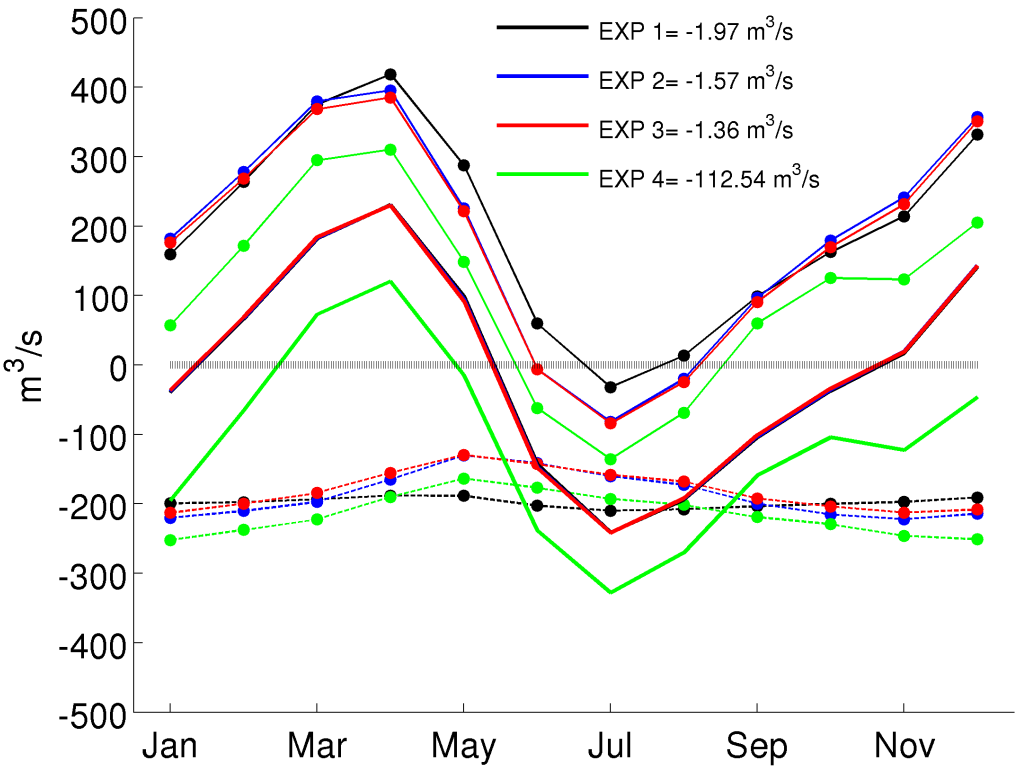

Figure 2.16: Seasonal variation of the net volume transport through sections 1T (dotted thin lines) and 3 (dot-dashed thin lines). The balance between those sections (1T plus 3) is represented by thicker lines. Results are month averaged (58 tidal cycles). Colors represent different experiments: EXP1 (black), EXP2 (blue), EXP3 (red) and EXP4 (green). And the legend values are the annual residual volume transport, negative is seaward.

only in March and April, and water export prevails through most of the year. The annual discharge budget equals to 112.5 m^3 s^{-1}, which is close to the annual average freshwater discharge of 124 m^3 s^{-1}.

Seasonal variation of the net volume transport through sections 1T (dotted thin lines) and 3 (dot-dashed thin lines). The balance between those sections (1T plus 3) is represented by thicker lines. Results are month averaged (58 tidal cycles). Colors represent different experiments: EXP1 (black), EXP2 (blue), EXP3 (red) and EXP4 (green). And the legend values are the annual residual volume transport, negative is seaward.

Flushing time

The results for the flushing time vary significantly between the experiments, and clearly show importance of the baroclinic forcing to the water-renewal capacity of the BTS. The

circulation forced exclusively by tides (EXP1) is not able to significantly flush the bay after 350 days of simulation (Figure 2.17), as the concentration does not fall below the e^{-1} (∼37%) threshold. Strong tidal flows coupled with a complex topography give rise to significant eddies as a result of sharp spatial changes in flow accelerations. Despite the improvement that eddies cause on dispersion (Zimmerman, 1986; Geyer and Signell, 1992), it does not further the flushing ability of the BTS. This can be ascribed to the dimensions of the bay in relation to the average tidal excursion (∼ 5 km). According to Geyer and Signell (1992), estuaries in which the typical spacing between major features is larger than the tidal excursion, only localized influence of tidal dispersion will exist, and this will not contribute to the overall flushing.

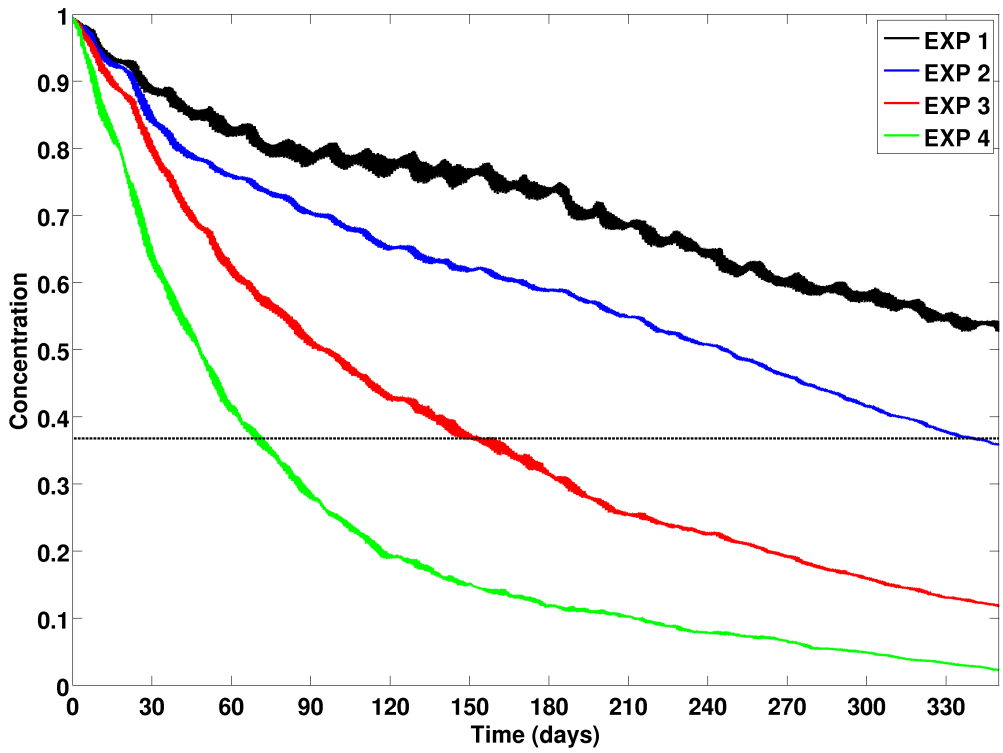

Figure 2.17: Time series of float concentration relative to the initial amount of drifters added in the fourth year of simulation inside the BTS. The colors black (EXP1), blue (EXP2), red (EXP3) and green (EXP4) represent the concentration of each experiment. The dotted line illustrates the e-folding mark.

The inclusion of the wind drag improved the flushing ability of the bay, (EXP 2) with an e-folding flushing time estimate of 340 days. A strong change occurs with the inclusion of the baroclinic effects of the heat and fresh water fluxes, as the e-folding flushing time is shortened to 147 days with the establishment of a gravitational circulation. The flushing time is reduced by a factor of 5 (68 days) in relation to EXP2 with the addition of the riverine discharge in the simulations. As presented before when the river discharge is included to the

simulation, a vertically-sheared flow is observed in the major part of the BTS, increasing the exchange of estuarine water with the shelf.

2.1.6 Summary and conclusions

The BTS is a tropical, tide-dominated, well-mixed estuary where the freshwater input switches from a strong point-source discharge in the summer (Paraguaçu River) to a more diffuse discharge related to atmospheric precipitation and small peripheral catchments in the fall and winter. East winds and a highly positive heat flux in the summer generate a steep positive gradient of water temperature towards the bay. This gradient is completely destroyed through the fall and winter when southeast winds prevail. The impact of this seasonality on the residual circulation and flushing time was investigated with ROMS numerical simulations.

The tide is the main driver of the residual circulation, generating eddies and significant advective accelerations close to narrows and headlands internal to the BTS. The tide residuals also produce a horizontally-sheared flow in the 2 control cross sections that regulate exchanges within the bay and between the bay and the ocean. Although little seasonal variability was observed in the tidally generated residual circulation, the tide was responsible for variations of the net-month water discharges between the bay and the shelf, forcing a water export between June and October. The tides alone, however, were not capable to reach an e-folding flushing time during the 350 days of simulation.

The wind drag was important to the surface circulation, forcing westbound (northbound) currents in the spring-summer (fall-winter) months and creating negative elevation gradients towards the sea. Although its impact in the overall residual circulation was small, with associated currents one order of magnitude smaller than the other forcing agents, the wind helped in regulating the net-month water discharges through the year, increasing the imports (exports) in the summer (winter) through Salvador Channel. It also showed significant importance in reducing the e-folding flushing time by at least 6 months in relation to the tide-only results.

The heat and water fluxes established an incipient gravitational circulation, i.e., vertically sheared flows with water ebbing on the surface, mainly due to large ($\sim$0.2 °C/km) temperature gradients in the summer. At these times the heat and water fluxes forced residual currents of similar, albeit smaller, magnitudes to the tide residuals. Their impact on the net water discharges was, however, rather small. The initial development of the gravitational circulation improved considerably the flushing ability of the bay, and the flushing time of the preceding model run (340 days) was more than halved to 147 days.

The river discharge was second to the tide in establishing the residual circulation in the BTS, and consolidated the gravitational circulation through most of the bay, including the Salvador Channel. The higher baroclinic pressure gradient generated by the river, in association with the barotropic pressure gradient, balanced both the horizontal advective accelerations and vertical viscosity in the more open areas of the bay away from topographic constrictions. The river discharge acting in concert with the heat and water fluxes reduced the e-folding flushing time by about 9 months (68 days) relative to the experiment with wind and tides.

The heat and water fluxes were surprisingly important to the residual circulation, establishing summer fluxes of equal magnitude to the river induced residual flow. The strongly positive heat flux appears to be more important than the positive (from the ocean to the atmosphere) water flux in the summer in defining the water density field. The temperature control on the density field has also been key to the flushing of hypersaline water in temperate semi-arid bays in Australia (De Silva Samarasinghe et al., 2003, Teixeira 2010), when lowering water temperatures stifle the inverse estuarine gravitational circulation in the autumn. Further numerical investigations will address the separate impacts of the heat and water fluxes on the residual circulation of the BTS.

The use of baroclinic tridimensional simulations allowed us to show that the impact of the baroclinic forcing on the circulation and flushing time is quite significant and must be taken into account in simulations aiming at the determination of pollutant and suspended sediment transport. Our results should also be taken into account on the management of the Paraguaçu River dam system, the largest catchment of the BTS.

Agradecimentos

Gostaria de agradecer, primeiramente, a Deus pela vida, a minha vó, ao meu pai e a minha mãe pelo suporte necessário ao longo da minha jornada na vida e na faculdade.

Aos meus orientadores, Guilherme Camargo Lessa e Carlos Teixeira, por terem acreditado no meu potencial e pelo grande aprendizado que obtive durante a elaboração desse trabalho.

A CAPES pelo financiamento da pesquisa.

Aos meus amigos de faculdade que estiveram sempre presentes para ajudar, discutir idéias, descontrair nos momentos de tensão e que foram personagens de épicas madrugadas de surfe.

Aos meus educandos, pela dedicação e contribuição substancial na minha ascenção como profissional.

Ao Programa de Pós-Graduação em Geofísica, pela oportunidade de crescer academicamente e realizar este trabalho.

Ao Grupo de Oceanografia Tropical (GOAT) que me acolheu e faz crescer a Oceanografia no Norte-Nordeste.

Em especial à minha namorada, Elissama Menezes, que mesmo à distância, emana amor, carinho, atenção, conversas, risos, gargalhadas e compreensão.

Referências Bibliográficas

Amorim, F. N.; Cirano, M.; Marta-Almeida, M.; Middleton, J. and Campos, E. J. D. (2013) The seasonal circulation of the Eastern Brazilian Shelf between 10°S and 16°S: A modelling approach, Cont. Shelf Res., **65**:121–140, doi:10.1016/j.csr.2013.06.008.

Barnier, B.; Siefridt, L. and Marchesiello, P. (1995) Thermal forcing for global ocean circulation model using a 3-year climatology of ECMWF analyses, J. Marine Syst., **6**:363–380.

Barros, F. C. R.; Cruz, I. C. S.; Kikuchi, R. K. P. and LeÃ£o, Z. M. A. N. (2009) BaÃa de Todos os Santos: aspectos oceanogrÃ¡ficos, chap. Ambiente BentÃ´nico, pp. 207 – 241, Vanessa Hatje, and Jailson B. de Andrade, Salvador - BR.

Bolaños, R.; Brown, J.; Amoudry, L. and Souza, A. (2013) Tidal, Riverine, and Wind Influences on the Circulation of a Macrotidal Estuary, JPO, **43**:29–50.

Cameron, W. M. and Pritchard, D. W. (1963) The Sea, chap. Estuaries, pp. 306 – 324, Hill, M. N., New York, USA.

Cirano, M. and Lessa, G. C. (2007) Oceanographic characteristics of Baía de Todos os Santos, Brazil, Revista Brasileira de Geofísica, **25**:363–387.

Cruz, I. C. S. (2008) Áreas prioritárias para conservação dos recifes de corais da Baía de Todos os Santos, Dissertação de Mestrado, Universidade Federal da Bahia, Bahia, Brasil, 102p.

De Silva Samarasinghe, J. R.; Bodeb, L. and Mason, L. B. (2003) Modelled response of Gulf St Vincent (South Australia) to evaporation, heating and winds, Cont. Shelf Res., **23**:1285–1313.

Delhez, E. J. M. (2013) On the concept of exposure time, Cont. Shelf Res., **71**:27–36.

Egbert, G. D.; Bennett, A. F. and Foreman, M. G. G. (1994) Efficient inverse modeling of barotropic ocean tides., J. Geophys. Res.-Oceans, doi: 10.1029/94JC01894.

Genz, F. (2006) Avaliação dos efeitos da Barragem de Pedra do Cavalo sobre a circulação estuarina do Rio Paraguaçu e BaíÃa de Iguape, Tese de Doutorado, Universidade Federal da Bahia, Bahia, Brasil.

Geyer, W. R. and Signell, R. P. (1990) Measurements of tidal flow around a headland with a shipboard acoustic doppler current profiler, J. Geophys. Res., **95**:3189–3197.

Geyer, W. R. and Signell, R. P. (1992) A reassessment of the role of tidal dispersion in estuaries and bays, Estuaries, **15**:97–108.

Gross, E. S.; Koseff, J. R. and Monismith, S. G. (1997) Threedimensional salinity simulations of south san francisco bay, J. Hydraul. Eng., **125**:1199–1209.

Haidvogel, D. B.; Arango, H.; Budgell, W. P.; Cornuelle, B. D.; Curchitser, E.; Di Lorenzo, E.; Fennel, K.; Geyer, W. R.; Hermman, A. J.; Lanerolle, L.; Levin, J.; McWilliams, J. C.; Miller, A. J.; Moore, A. M.; Powell, T. M.; Shchepetkin, A. F.; Sherwood, C. R.; Signell, R. P.; Warner, J. C. and Wilkin, J. (2008) Ocean forecasting in terrain-following coordinates: Formulations ans skill assesment of the Regional Ocean Modeling System, J. Comput. Phys., **227**:3595–3624.

Hatje, V. and De Andrade, J. B. (2009) Baía de Todos os Santos: aspectos oceanográficos, Editora da Universidade Federal da Bahia, Bahia, Brasil.

HYCOM (2011) Consortium for Data Assimilative Modeling - HYCOM+NCODA Global Analysis, disponível em: http://www.hycom.org/dataserver/glbanalysis/.

IBGE (2013) Instituto brasileiro de geografia e estatística - rede maregráfica permanente para geodésia - rmpg, disponível em: http://www.ibge.gov.br/home/geociencias/geodesia/rmpg/rmpg_est.shtm.

IBGE (2014) Instituto brasileiro de geografia e estatística - estimativas populacionais para os municípios brasileiros, disponível em: http://www.ibge.gov.br/home/estatistica/populacao/estimativa2013/estimativa_tcu.shtm.

INMET (1992) Normas Climatológicas - 1961 a 1990, Ministério da Agricultura, Pecuária e Abastecimento, 155 pp.

Kanamitsu, M.; Ebisuzaki, W.; Woollen, J.; Yang, S.; Hnilo, J. J.; Fiorino, M. and Potter, G. L. (2002) NCEPDOE AMIP-II Reanalysis (R-2), Bull. Am. Meteorol. Soc., **83**:1631–1643.

Kantha, L. H. and Clayson, C. A. (1994) An improved mixed layer model for geophysical applications, J. Geophys. Res., **99**:25235–25266.

Lessa, G. C.; Bittencourt, A. C. S. P.; Brichta, A. and Dominguez, J. M. L. (2000) A reevaluation of the late quaternary sedimentation in todos os santos bay, brazil, in: *Anais da Academia Brasileira de Ciências*, vol. 72, pp. 573–590.

Li, C. and O'Donnell, J. (2005) The effect of channel length on the residual circulation in tidally dominated channels, J. Phys. Oceanogr., **35**:1826–1840.

Li, Y. and Li, M. (2012) Wind-driven lateral circulation in a stratified estuary and its effects on the along-channel flow, J. Geophys. Res.

Marchesiello, P.; McWilliams, J. C. and Shchepetkin, A. F. (2001) Open boundary conditions for long-term integration of regional oceanic models, Ocean Modelling, **3**:1–20.

Meyers, S. D. and Luther, M. E. (2008) A Numerical Simulation of Residual Circulation in Tampa Bay Part II: Lagrangian Residence Time, Estuar Coast, **31**:815–827.

Miranda, L. B.; Castro, B. M. and Kjerfve, B. (2002) PrincÃpios de Oceanografia FÃsica de EstuÃ¡rios, Editora da Universidade de SÃ£o Paulo, 414p.

Pawlowicz, R.; Beardsley, B. and S., L. (2002) Classical tidal harmonic analysis including error estimates in matlab using t_tide, Computers and Geosciences, **28**:929–937.

Pereira, M. G. and Lessa, G. C. (2009) Varying patterns of water circulation in Canal de Cotegipe, Baía de Todos os Santos, Revista Brasileira de Geofísica, **27**(1):1–17.

Pritchard, D. W. (1955) Estuarine circulation patterns, in: *Proceedings of Am Soc Civil Eng.*

Pugh, D. T. (1987) Tides, Surges and Mean Sea Level, Wiley, Chichester, 472p.

Reyes, A. C. and Valle-Levinson, A. (2010) Wind modifications to density-driven flows in semienclosed, rotating basins, J. Phys. Oceanogr., **40**:1473–1487.

Ribeiro, C. H. A.; Waniek, J. J. and Sharples, J. (2004) Observations of the spring-neap modulation of the gravitational circulation in a partially mixed estuary, Ocean Dynamics, **54**:299–306.

Saha, S. and Coauthors (2010) The NCEP Climate Forecast System Reanalysis, Bull. Am. Meteorol. Soc., **91**:1015–1057, doi: 10.1175/2010BAMS3001.1.

Scully, M. E.; Geyer, W. R. and Lerczak, J. A. (2009) The Influence of Lateral Advection on the Residual Estuarine Circulation: A Numerical Modeling Study of the Hudson River Estuary, J. Phys. Oceanogr., **39**:107–124, doi: 10.1175/2008JPO3952.1.

Shchepetkin, A. F. and McWilliams, J. C. (2003) A method for computing horizontal pressure-gradient force in an oceanic model with a non-aligned vertical coordinate, J. Geophys. Res., **108**:1–34.

Shchepetkin, A. F. and McWilliams, J. C. (2005) The regional ocean modeling system: A split-explicit, free-surface, topography following coordinates ocean model, Ocean Modelling, **9**:347–404.

Simpson, J. H.; Brown, J.; Matthew, J. and Allen, G. (1990) Tidal straining, density currents, and stirring in the control of estuarine stratification, Estuaries, **13**:125–132.

Souto, C.; Gilcoto, M.; Fariña Busto, L. and F., P. F. (2003) Modeling the residual circulation of a coastal embayment affected by wind-driven upwelling: Circulation of the rÃa de vigo (nw spain), J. Geophys. Res., doi:10.1029/ 2002JC001512.

Takeoka, H. (1984) Fundamental concepts of exchange and transport time scales in a coastal sea, Cont. Shelf Res., **3**:311–326.

Teixeira, C. E. P. (2010) Ocean Dynamics of Spencer Gulf: a numerical study Dissertation, University of New South Wales, Ph.D. thesis, University of New South Wales.

Thomann, R. V. and Mueller, J. A. (1987) Principles of Surface Water Quality Modelling and Control, Harper Collins, New York.

Umlauf, L. and Burchard, H. (2003) A generic length-scale equation for geophysical turbulence, J. Mar. Res., **61**:235–265.

Verspecht, F.; Rippeth, T. P.; Simpson, J. H.; J., S. A.; Burchard, H. and Howarth, M. J. (2009) Residual circulation and stratification in the liverpool bay region of freshwater influence, Ocean Dynamics, **59**:765–779.

Weisberg, R. H. and Zheng, L. Y. (2006) Circulation of tampa bay driven by buoyancy, tides, and winds, as simulated using a finite volume coastal ocean model, J. Geophys. Res., doi:10.1029/2005JC003067.

Winant, C. D. (2004) Three dimensional wind-driven flow in an elongated, rotating basin, J. Phys. Oceanogr., **34**(462–476).

Xavier, A. G. (2002) Análise hidrodinâmica da Baía de Todos os Santos, Ph.D. thesis, Programa de Pós-Graduação em Engenharia, UFRJ, 222 pp.

Zheng, L. Y. and Weisberg, R. H. (2004) Tide, buoyancy, and wind-driven circulation of the charlotte harbor estuary: A model study, J. Geophys. Res., doi:10.1029/2003JC001996.

Zimmerman, J. T. F. (1978) Topographic Generation of Residual Circulation by Oscillatory (Tidal) Currents, "Geophys. Astrophys. Fluid Dyn", **11**:35–47.

Zimmerman, J. T. F. (1986) The tidal whirlpool: A review of horizontal dispersion by tidal and residual currents, "J Sea Res", **20**:133–154.